Properties of the Hα-emitting Circumstellar Regions of Be Stars

Christopher Tycner,[1,2,3] John B. Lester,[4] Arsen R. Hajian,[5] J. T. Armstrong,[6] J. A. Benson,[1] G. C. Gilbreath,[6] D. J. Hutter,[1] T. A. Pauls,[6] N. M. White[7]

tycner@nofs.navy.mil; lester@astro.utoronto.ca; hajian@usno.navy.mil; tom.armstrong@nrl.navy.mil; jbenson@nofs.navy.mil; Charmaine.Gilbreath@nrl.navy.mil; djh@nofs.navy.mil; pauls@nrl.navy.mil; nmw@lowell.edu

arXiv:astro-ph/0501552v1 25 Jan 2005

ABSTRACT

Long-baseline interferometric observations obtained with the Navy Prototype Optical Interferometer of the Hα-emitting envelopes of the Be stars η Tauri and β Canis Minoris are presented. For compatibility with the previously published interferometric results in the literature of other Be stars, circularly symmetric and elliptical Gaussian models were fitted to the calibrated Hα observations. The models are sufficient in characterizing the angular distribution of the Hα-emitting circumstellar material associated with these Be stars. To study the correlations between the various model parameters and the stellar properties, the model parameters for η Tau and β CMi were combined with data for other Be stars from the literature. After accounting for the different distances to the sources and stellar continuum flux levels, it was possible to study the relationship between the net Hα emission and the physical extent of the Hα-emitting circumstellar region. A clear dependence of the net Hα emission on the linear size of the emitting region is demonstrated

[1]US Naval Observatory, Flagstaff Station, P.O. Box 1149, Flagstaff, AZ 86002-1149

[2]NVI, Inc., 7257 Hanover Parkway, Suite D, Greenbelt, MD 2077011

[3]Also Department of Astronomy and Astrophysics, University of Toronto, Toronto, ON, Canada

[4]Department of Astronomy and Astrophysics, Erindale Campus, University of Toronto, 3359 Mississauga Road North, Mississauga, ON L5L 1C6, Canada

[5]US Naval Observatory, 3450 Massachusetts Avenue, NW, Washington, DC 20392-5420

[6]Remote Sensing Division, Code 7210, Naval Research Laboratory, 4555 Overlook Avenue, SW, Washington, DC 20375

[7]Lowell Observatory, 1400 West Mars Hill Road, Flagstaff, AZ 86001

and these results are consistent with an optically thick line emission that is directly proportional to the effective area of the emitting disk. Within the small sample of stars considered in this analysis, no clear dependence on the spectral type or stellar rotation is found, although the results do suggest that hotter stars might have more extended Hα-emitting regions.

Subject headings: stars: emission-line, Be — techniques: interferometric

1. Introduction

Over the years, numerous observational and theoretical studies have shown that nearly all stars lose mass in the form of stellar winds. Although the details associated with the wind formation can be quite different from one star to another, and could involve a number of different physical processes, the most common driving force is the stellar radiation field. In fact, the radiation alone can be responsible for driving the stellar wind as the photons are absorbed or scattered by the outflowing material. In cool stars, where the conditions in the wind permit dust to form, the photons are absorbed by the dust particles, while in hotter stars the photon momentum is transferred to the wind by excitation of the atomic gas, resulting in what is known as line-driven wind.

Among the B-type stars, which have effective temperatures in the range of 10,000 to 30,000 K, there exists a very interesting class of stars that possess circumstellar regions with much higher densities than expected for line-driven winds of stars of similar effective temperatures and masses. These stars are known as Be stars and their common characteristic is that they have, or had in the past, at least one Balmer line in emission. Typically, the Be notation is reserved for non-supergiant B-type stars with line-emitting circumstellar material. It is sometimes necessary to emphasize the difference between Be stars with circumstellar envelopes that are thought to be formed by an outflowing material and B-type stars with circumstellar regions that are formed by accretion of the surrounding material, as in the case of Herbig Ae/Be stars, or semi-detached (Algol type) binary systems. In such case, the term "classical Be star" is used to explicitly identify non-accreting B-type stars with circumstellar regions (see also the review paper by Porter & Rivinius 2003).

The initial attempts to apply optical interferometry to Be stars have been quite promising. Thom, Granes, & Vakili (1986) were the first to spatially resolve the the circumstellar envelope of a Be star (γ Cas) using the I2T interferometer. Shortly thereafter, the Mark III interferometer was used to obtain the first direct measurements of the deviation from spherical symmetry of the Hα-emitting regions of γ Cas and ζ Tau (Quirrenbach et al. 1993, 1994). Interferometric observations that divide the Hα emission line into a number of spectral channels have also been obtained with the GI2T interferome-

ter, and they resulted in the first detection of a rotational signature in an envelope of a Be star (Mourard et al. 1989; Stee et al. 1995). The combination of linear polarization studies with interferometric observations of a number of Be stars, which have shown that the Hα-emitting envelopes are flattened, is the strongest observational evidence to date for the presence of relatively thin circumstellar disks (Quirrenbach et al. 1997).

The recent interferometric detection of a high degree of oblateness of the stellar photosphere in the Be star α Eridani by Domiciano de Souza et al. (2003), compounded with the possibility that most $v \sin i$ values for Be stars could be significantly underestimated (Townsend, Owocki, & Howarth 2004), has reignited the interest in the connection between the stellar rotation and the Be disk formation mechanisms. Similarly, the study of the correlation between the strength of the Hα emission line and the spatial extent of the emitting region of a Be star can be used to establish the properties of the circumstellar region. Although Quirrenbach et al. (1997) have shown that there is a tendency for stars with larger disks to have stronger Hα emission, there was also a considerable scatter present in their results. We will extend their analysis to account for the different base flux levels in the Hα emission lines, and we will show that there is a clear relationship between the net emission and the physical extent of the Hα-emitting disk.

2. Initial Reductions and Calibration

The new observations that we present in this paper, as well as those that were reported previously (Tycner et al. 2003, 2004), were all obtained with the Navy Prototype Optical Interferometer (NPOI). The instrument is a descendant of the Mark I through Mark III phase-tracking optical interferometers (Shao & Staelin 1980; Shao et al. 1987, 1988) and is located at the dark observing site of the Lowell Observatory, near Flagstaff, Arizona. We will review here only those aspects of the instrument and the observational setup that are directly relevant to the work presented in this paper. For a more detailed discussion of the instrument, the initial data reduction process, and the calibration, the reader is referred to the papers by Armstrong et al. (1998), Hummel et al. (1998), and Tycner et al. (2004), respectively.

The NPOI consists of an imaging and an astrometric array, but for all the NPOI observations discussed in this paper only three astrometric stations located in the inner part of the array were used (also referred to as the AC0, AE0, and AW0 stations; Armstrong et al. 1998). The three baselines formed by the AC0–AE0–AW0 triangle are shown in Figure 1 with dotted lines. Each pair of elements creates an interference pattern at the beam combiner, which is then dispersed by a prism onto a lenslet array. A series of optical fibers that are glued to the back of each of the three lenslet arrays carry the signal to a cluster of photon-counting avalanche photodiodes (APDs), which record the intensity variations as a function of a variable optical path difference. Each lenslet

array provides 32 spectral channels covering the 450–850 nm spectral region. However, because the number of available APDs was limited at the time of observations, as well as the signal-to-noise ratio (SNR) was too low in some channels (especially those at shorter wavelengths where the sensitivity of the instrument is low), not all spectral channels were usable. Also, the spectral alignment of the lenslet arrays was such that the Hα emission was located in one of two spectral channels depending on the baseline (i.e., depending which lenslet array detected the signal for that baseline). These two channels are labeled with central wavelengths of 648 and 665 nm, but because both of these channels have approximately the same spectral width of 16 nm, the ones that contain the Hα emission line are referred to as the Hα channels (see also Tycner et al. 2004, where the alignment of the spectral channels is described in detail).

We obtain an estimate of squared visibility for every 2 ms data frame, and these values are then incoherently averaged over 1 s intervals to create 1 s data points (see Hummel et al. 1998, for more details). In a subsequent step a raw squared visibility that corresponds to a 90 s interval (known also as a "scan") is calculated by a simple average. In the process, the observational errors of the raw scans are set equal to the standard deviation of the 1 s data points divided by the square root of the number of points in a scan. This approach produces larger errors than one would get by propagating the errors of the individual 1 s data points (Hummel et al. 1998), but it is part of the standard reduction scheme that attempts to account for both the white and the non-white noise sources (i.e., it attempts to account for some of the atmospheric and instrumental effects). If some of these effects are removed from the data through subsequent calibration (like the one we developed in Tycner et al. 2003), these error bars will tend to overestimate the magnitude of the actual observational uncertainties. New methods for estimating the interferometric observables along with their associated uncertainties are currently being developed by the NPOI team, but their discussion is beyond the scope of this paper.

2.1. Observations of η Tauri and β Canis Minoris

The Be stars η Tauri (=HR 1165) and β Canis Minoris (=HR 2845) have been observed with the NPOI on many occasions, although most of the time not as primary scientific targets. In many instances they have been used as calibration sources, or check stars for observations of other targets, frequently binary systems. This resulted in a quite limited coverage of these stars on any single night, but searching through the archival observations of NPOI we have found 22 nights from late 1997 to early 1999 that contained at least some valid scans of η Tau or β CMi. Some scans were excluded because of missing data on one of the baselines, or very low SNR due to poor atmospheric conditions. Table 1 lists the dates and the number of scans of η Tau and β CMi available for analysis from each of the 22 nights.

We begin by calibrating the V^2-values of η Tau and β CMi using exactly the same method as was used in the case of ζ Tau (Tycner et al. 2004). For the stellar disk diameters of η Tau and β CMi we adopt the photometrically inferred values of 0.71 and 0.74, respectively (Quirrenbach et al. 1997). Because the instrumental configuration of the NPOI was unchanged, for all practical purposes, from 1997 until mid-1999, the spectral alignment of the output beams with respect to the lenslet arrays was the same for all stars observed with the NPOI over that period. Also, as it was discussed in Tycner et al. (2004), the alignment of the spectral channels was such that the Hα emission was located in either the 648 or 665 nm channel, depending on the baseline. We verify if this is also the case for η Tau and β CMi by comparing the signal from the channels that are expected to contain the Hα signal with those that do not.

The calibrated squared visibilities of η Tau from the Hα-containing channels are shown in Figure 2 along with the V^2-values for the uniform disk (UD) model representing the stellar photosphere. The squared visibilities from the Hα channels systematically fall below the expected photospheric values, especially at the higher spatial frequencies. We interpret this as a direct signature of a resolved circumstellar envelope that is responsible for the Hα emission. Figure 3 demonstrates that the signature in the 648 and 665 nm channels without the Hα emission, is very similar to that seen in the continuum channels at both shorter (Fig. 4), and longer (Fig. 5) wavelengths. Although the quantity of data is much smaller in the case of β CMi, the same conclusions can be reached by inspecting the signal in the spectral channels with and without the Hα emission (see Figs. 6 and 7). Based on this we conclude that all of the Hα emission is captured in one spectral channel at all three baselines for both η Tau and β CMi.

2.2. Modeling the Hα-emitting Envelopes

The interferometric observations of Be stars represent a unique class of observations, where the star can be modeled with a simple two-component model. At the angular resolution provided by our observations the stellar photosphere, which is visible at the continuum wavelengths, can be modeled with the UD model. The second component, which is responsible for the Hα emission, can be modeled with an elliptical Gaussian to determine the angular extent and the ellipticity of the circumstellar region. If the two components are assumed to be concentric, then the net squared visibility for both components can be expressed as a normalized sum of the form:

$$V^2_{\rm UD+Gauss} = \left[c_{\rm p} V_{\rm UD}(\theta_{\rm UD}) + (1 - c_{\rm p}) V_{\rm Gauss}(\theta_{\rm mj}, r, \phi)\right]^2 , \qquad (1)$$

where both $V_{\rm UD}(\theta_{\rm UD})$ and $V_{\rm Gauss}(\theta_{\rm mj}, r, \phi)$ are discussed in detail in Tycner et al. (2004). The $c_{\rm p}$ parameter in the above equation represents the net fractional contribution from the stellar photosphere to the net signal in the Hα channel, and, because it is defined to

have a value between 0 and 1, it also maintains the normalization of the net visibility. Of course, if the two components are not concentric then the individual visibility amplitudes cannot be added in such a simple way and one would have to account for the relative complex phase shifts between the models. However, because our observations were obtained at a relatively short baselines (18.9–37.5 m), we resolve only the overall shape of the circumstellar regions and we are insensitive to small scale deviations from point-symmetric source structure.

To be consistent with the modeling of the Hα-emitting envelopes of γ Cas and ζ Tau (Tycner et al. 2003, 2004), we model the envelopes of η Tau and β CMi using Gaussian models. We first fit a circularly symmetric Gaussian to the data by keeping the axial ratio, r, fixed at unity and the resulting two-parameter fits are listed in Table 2. As expected, because both stars have a relatively weak Hα emission, the contribution from the stellar photosphere to the net signal in the Hα channel is large in both cases (roughly 90%). The best-fit circularly symmetric Gaussian model for η Tau is shown in Figure 2 along with the resulting normalized residuals. The majority of the data points do not deviate from the model by more than one standard deviation, although the residuals in Figure 2 (which have a χ^2_ν of 1.03) show more variation than the residuals calculated from the difference between the UD model and the data in the continuum channels (see the residuals in Figs. 3, 4, and 5 which have χ^2_ν values of 0.83, 0.57, and 0.43, respectively). Likewise the best-fit circularly symmetric Gaussian model for β CMi is shown in Figure 6.

Fitting elliptical Gaussian models to the squared visibilities from the Hα channels of η Tau and β CMi yields model parameters with an apparent ellipticity in both cases. The model parameters are listed in Table 2 along with the corresponding χ^2_ν values, which also suggest that the elliptical Gaussian models result in a slightly better fits. Unfortunately, we cannot confidently rule out the possibility that the apparent ellipticity is a result of systematic errors that could be present in our data (for example due to insufficient bias level corrections). However, it is interesting to note that Quirrenbach et al. (1997), who observed η Tau and β CMi with the Mark III interferometer (and thus were influenced by different systematic errors), reported similar model parameters for both stars.

3. The Data

The modeling presented in this paper and Tycner et al. (2003, 2004) has resulted in properties of Hα-emitting envelopes for a total of four Be stars that have been observed with the NPOI. Because we model each Hα-emitting envelope in nearly the same way as Quirrenbach et al. (1997), we can also include their results for three extra Be stars to increase the sample size. Table 3 lists the names and the spectral types (from the Bright Star Catalogue, BSC, Hoffleit & Jaschek 1982) of the Be stars observed with the NPOI, along with those that have model parameters based on the work of Quirrenbach et al.

(1997), at the bottom of the list. We see from the table that we have a range of spectral types, and thus it should be possible to investigate not only the relationship between the Hα emission and the physical extent of the emitting region, but also to test for any obvious dependencies on spectral type. We begin by discussing the sources of the observational parameters derived from both interferometric and spectroscopic observations of each star.

For the Be stars γ Cas, η Tau, ζ Tau, and β CMi, best-fit model parameters describing an elliptical Gaussian model have been presented in Tycner et al. (2003, 2004) and § 2.2. The model parameters that are relevant to our discussion are the angular size of the major axis ($\theta_{\rm mj}$) and the ratio of the minor to major axis (r). Quirrenbach et al. (1997) also obtained the same model parameters for ϕ Per, ψ Per, and 48 Per and therefore in Table 3 we adopt their parameters for these stars.

The radiation from the circumstellar disk of a Be star can be characterized by the equivalent width (EW) of the Hα emission line. Unfortunately, our interferometric observations do not contain this type of detailed spectroscopic information, and thus we need to rely on independently obtained spectroscopic observations. For Be stars that are known to possess Hα emission that is stable on long time scales, it is not necessary to obtain spectra that cover the same time-frame as the interferometric observations. On the other hand, for stars whose variability is well documented, spectroscopic observations taken as close in time as possible to the interferometric observations are required. We have searched the literature for spectroscopic information on the Hα emission that would cover the same period as our interferometric observations, which were acquired between 1997 and 1999, and those of Quirrenbach et al. (1997), which were obtained throughout 1992.

To check for consistency and long-term stability of the Hα emission of the targets observed with the NPOI, we have obtained echelle spectra of γ Cas and ζ Tau on 2003 December 9, and η Tau and β CMi on 2004 March 8. The echelle spectra were obtained using the Lowell Observatory's Solar-Stellar Spectrograph (SSS) located at the same site as the NPOI. The SSS instrument and the IDL-based reduction package that was used to extract the spectra from the raw echelle orders were described by Hall et al. (1994). The resulting spectra of the Hα region, shown in Figure 8, have a resolving power of about 30,000 and SNR in the range of 150–200 at the continuum wavelengths, and higher at the emission line.

3.1. Hα emission of η Tau and β CMi

The Hα emission profiles of η Tau and β CMi are presented in the literature for a number of different epochs. By inspecting the profiles obtained by various observers between 1980 and 1999 (Andrillat & Fehrenbach 1982; Slettebak, Collins, & Truax 1992;

Hanuschik et al. 1996; Banerjee et al. 2000), as well as the profiles from 2004 shown in Figure 8, we conclude that the overall emission remained largely unchanged for both stars over the period covered by the observations. This is true not only for the relative shape of the line but also the width and the peak intensity. The only exception are the observations reported by Banerjee et al. (2000), where the emission appears higher above the continuum (by ∼10 and ∼30 % for β CMi and η Tau, respectively) than in all other references. Because Banerjee et al. (2000) have a spectral coverage of approximately 2.5 nm centered on Hα, which is narrower than the full extent of the underlying absorption line, their Hα profiles are susceptible to incorrect normalization of the continuum level when the absorption line is not completely filled in (as is the case in η Tau and β CMi). Treating the extended wings of the absorption component as the continuum level will then result in an overestimation of the peak intensity of the emission component. Therefore, we conclude that the Hα profiles of η Tau and β CMi do not change significantly on long time scales and for these two stars we use the equivalent widths of the emission lines observed in 2004, shown in Figure 8.

3.2. Hα emission of γ Cas and ζ Tau

Both γ Cas and ζ Tau are known to show complex variations in their Hα emission profiles on time scales from months to years, but in both cases the variations on the longer time scales are always more significant. Furthermore, because the EW measure is an integrated quantity, it has the tendency to be insensitive to the small-scale variations in the line profile, typically seen at the shortest time scales. Therefore we are only interested in the changes in the EW of Hα on the time scales of years.

In the case of γ Cas the spectroscopic observations conducted by Banerjee et al. (2000) are the closest in time to our interferometric observations that were obtained between 1997 and 1998 (Tycner et al. 2003). Banerjee et al. (2000) reports Hα EW of -2.25 nm at the end of 1998, and -2.67 nm for observations obtained a year later. By comparing the above values with the EW of -2.57 nm that we obtain for the Hα profile of γ Cas from 2003 (recall Fig. 8), we conclude that variability in the EW at the ∼20% level, on time scale of a year, can be expected. However, because the observations of Banerjee et al. (2000) from 1998 were acquired only one month after our 1998 interferometric observations, we use their reported EW of Hα as the corresponding emission measure for our observations.

The interferometric observations of ζ Tau that we have analyzed in Tycner et al. (2004) were obtained on 1999 March 1. Once again, the Hα observations by Banerjee et al. (2000) conducted on 1999 March 16 are the closest in time to our observations. Because the Hα profile variations on time scales of days are very small in ζ Tau (Hanuschik et al. 1996), the EW of -2.06 nm reported by Banerjee et al. (2000) is suitable for our analysis.

It is also interesting to note that this value is effectively the same as the EW of −2.09 nm we obtain for the profile shown in Figure 8. We should also note that in the case of γ Cas and ζ Tau the Hα emission completely fills in the underlying absorption component and therefore the normalization of the continuum in these stars is less susceptible to errors, like the ones discussed in the previous section.

3.3. Hα emission of ϕ Per, ψ Per, and 48 Per

By comparing the Hα profiles of ϕ Per, ψ Per, and 48 Per from 1980 (Andrillat & Fehrenbach 1982), 1989 (Slettebak, Collins, & Truax 1992), 1993 (Hummel & Vrancken 1995), and 1998–2000 (Banerjee et al. 2000), we conclude that only ϕ Per has significantly varying Hα emission, but even in that case the main variation is a gradual weakening of the emission over many years. Since the Mark III observations of the above stars date back to 1992, we use the EW of Hα reported by Hummel & Vrancken (1995), who observed these stars in 1993. The three stars, ϕ Per, ψ Per, and 48 Per, have shown equivalent widths of −3.50, −3.37, and −2.23 nm, respectively.

4. The Analysis

4.1. Physical Extent of a Circumstellar Region

Because distance has a direct effect on angular size, the angular measurements of the major axes of the circumstellar regions must be either transformed into physical sizes (if the distances are known) or normalized with respect to the angular diameters of the central stars (which must be estimated since they have not been measured directly). The latter method was used by Quirrenbach et al. (1997), and, although it does eliminate the dependence on distance, it introduces a dependence on the size of the central star. Because we have a range of spectral types, this approach is not optimal.

A much better approach is to use the known distances to obtain directly the physical extent of each region. We use the observed Hipparcos parallax (π) to derive the corresponding distance (d) to each star. This in turn allows us to convert the best-fit value for the angular size of the major axis of the elliptical Gaussian model into a corresponding size in meters. Table 3 lists the angular size of the major axis ($\theta_{\rm mj}$) of each Hα-emitting region and the corresponding physical size in meters ($D_{\rm mj}$), along with the Hipparcos data used to calculate the distance to each star.

4.2. The Net Hα Emission

The equivalent widths of the Hα emission lines typically reported in the literature only measure the amount of emission above the continuum level. Because B-type stars possess significant Hα absorption profiles, we need to correct for the "filling-in" effect of the absorption line to recover the total amount of emission. In our approach we assume that the entire absorption line is filled in by the superimposed emission. This is a good approximation for the sources considered here, where the Hα emission lines are stronger and wider than the underlying absorption lines. Even in the case of η Tau and β CMi, where the absorption lines are not completely filled in (recall Fig. 8), the above assumption can still be applied, because our EW measures of the emission are already reduced by the amount the absorption line is not filled in.

To obtain an estimate on the EW of the absorption line, we follow the procedure developed by Coté & Waters (1987), who modeled the relationship between the EW of the Hα absorption line and the intrinsic $(B-V)_0$ color index for normal main sequence B-type stars. This can be done because in B-type stars the strength of the Hα absorption line increases monotonically with spectral type to a maximum at type A0. We should also note that for stars in our sample that are not on the main sequence, the equivalent widths of the absorption lines derived using the above method will be slightly overestimated (by not more than 0.1 nm). Because this is at the same level as the intrinsic scatter observed in the Hα equivalent widths for stars of the same spectral type (see, for example, Fig. 1 in Coté & Waters 1987), we neglect this overestimation in our analysis.

In Table 4 we list the observed $B-V$ colors from the BSC for each of the stars. Deriving the intrinsic $(B-V)_0$ color of the central star from the observed $B-V$ value is not trivial, even if the corrections for the interstellar extinction are known, because Be stars can still appear intrinsically redder than normal B-type stars of the same spectral type. This is typically attributed to free-bound and free-free emission, as well as a possible circumstellar reddening (Schild 1978). For this reason we estimate the $(B-V)_0$ index based on the spectral type and not on the observed $B-V$ color. Table 4 lists the $(B-V)_0$ values based on the tabulation of FitzGerald (1970) which in turn is used to calculate the equivalent widths of the Hα absorption lines (via eq. 6 of Coté & Waters 1987). These values are then combined with the equivalent widths of the observed Hα emission lines ($W_{\rm H\alpha}$) to give a measure of the net Hα emission ($E_{\rm H\alpha}$) from each circumstellar region (both quantities are listed in Table 6).

4.3. The Hα Luminosity

The net Hα emission derived in previous section, although corrected for the "filling-in" effect of the absorption line, is still measured with respect to the underlying stellar

continuum. Because we are dealing with spectral classes ranging from B0 to B8, we need to account for the different continuum flux levels. We use two independent methods to estimate the stellar continuum level. One method is based on the photometry and thus requires us to account for the different distances to the sources. The other method, which is distance independent, uses model energy distributions to represent the underlying stellar continuum. Because the second method does not account for the continuum emission from the circumstellar region, as well as requires an estimate of the stellar radius, it is only used to verify the photometrically derived results.

4.3.1. Hα luminosity based on photometrically determined continuum

Obtaining the flux levels of the individual stars from photometry is complicated by the interstellar extinction. Using the observed $B-V$ color and the estimated intrinsic $(B-V)_0$ color based on the spectral type, we can derive the color excess $E(B-V)$. This approach should work for the later type Be stars, but will tend to overestimate the color excess (by possibly as much as 0.15 mag) for spectral types B3e and earlier, because of the intrinsic reddening due to the free-bound and free-free emission from the circumstellar envelope (Schild 1978, 1983). Fortunately, there are other methods that can be used to estimate the color excess due to the interstellar extinction. For example, Beeckmans & Hubert-Delplace (1980) used the depth of the interstellar absorption bump at 2200 Å to derive the values of $E(B-V)$ for a number of Be stars and in Table 4 we list their values of $E(B-V)$ for all but two of our stars. The two missing Be stars are η Tau and β CMi, and because these stars have the latest spectral type, as well as being the closest, we simply derive an estimate of $E(B-V)$ based on their observed $B-V$ colors and the intrinsic $(B-V)_0$ colors derived from the spectral type.

With a known color excess $E(B-V)$ we can correct the apparent V magnitude of each star for interstellar extinction using:

$$V_0 = V - A_V = V - R_V \cdot E(B-V), \tag{2}$$

where R_V is the reddening constant, defined as $A_V/E(B-V)$. The typical value of R_V found by Schultz & Wiemer (1975) is 3.14±0.10. Similarly, the observed $V-R$ colors (see Table 4) can be corrected for interstellar reddening using the ratio of $E(V-R)/E(B-V) = 0.78 \pm 0.02$ derived by Schultz & Wiemer (1975), and in turn the R_0 magnitudes can be obtained. The R-band has an effective central wavelength of ∼658 nm and a FWHM of ∼138 nm, and thus R_0 magnitude can be used to measure the continuum flux level in the Hα region. Also, the relatively large spectral width of the R-band allows us to neglect the contribution of the Hα emission to R_0.

To convert a R_0 magnitude into a corresponding flux above Earth's atmosphere ($f_\star$)

we use

$$f_\star = f_{\rm s} 10^{-0.4(R_\star - R_{\rm s})}, \tag{3}$$

where $f_{\rm s}$ and $R_{\rm s}$ are the mean flux density (in the R-band) and the R magnitude of a standard star, respectively. Because we are interested in the functional dependence of the net Hα emission on the disk size, the actual value of $f_{\rm s}$ is not important. Nevertheless, in order to work with values that have physically meaningful units we use a *representative* value for the absolute flux density of $f_{\rm s} = 1.76 \times 10^{-11}$ W m^{-2}nm^{-1} defined for a standard star with $R_{\rm s} = 0$ (Johnson 1966). The values for $f_\star$ based on the R_0 magnitudes are listed in Table 5, along with the corresponding *total* radiation at Hα ($4\pi d^2 f_\star$).

Finally to work with an Hα emission measure that is independent of distance we multiply the net Hα emission, $E_{\rm H\alpha}$, derived in previous section, by the total radiation in the Hα region, to obtain

$$L_{\rm H\alpha} = 4\pi d^2 f_\star E_{\rm H\alpha}, \tag{4}$$

which we refer to as the Hα luminosity. The values for the Hα luminosities are given in Table 6 along with their corresponding uncertainties, which account for the errors in the distance determination (largest source of uncertainty), photometry, and the Hα equivalent widths, but do not include the uncertainty associated with the determination of the absolute flux density of a standard star.

4.3.2. Hα luminosity based on synthetic spectra

Instead of using photometry to derive the stellar continuum flux level in the Hα region, we can use synthetic spectra calculated for atmospheric models of varying effective temperatures. For this purpose we have used the well known grid of stellar atmosphere model spectra computed using the ATLAS9 program (Kurucz 1993). The models were chosen to have effective temperatures that were the same as, or as close to those estimated based on the spectral type (see Table 5). Because the grid covered the range of the effective temperatures in approximately 500 and 1,000 K steps, for some stars it was necessary to interpolate the fluxes in effective temperature. All models correspond to solar abundances, $\log g$ of 4 (for luminosity class V or IV) and 3.5 (for luminosity class of III), although little variation between the two gravities is present, and the standard microturbulence of 2 km s^{-1} was used. Figure 9 illustrates a sample of the physical flux ($\mathcal{F}_\star$) as a function of wavelength obtained for a 12,000 K model.

To estimate the total stellar radiation from the physical flux in the Hα region we need to account for the surface area of each star. We estimate the radius of each star based on its spectral type (Underhill et al. 1979), and the resulting synthetic total radiation in the Hα region ($4\pi R_\star^2 \mathcal{F}_\star^{\rm S}$) is given in Table 5. It is evident from the table that the synthetic values are systematically smaller than the photometrically derived ones, and

this should be expected because the synthetic spectra do not account for the bound-free and free-free emission from the circumstellar material. Although there does exist a general correlation between the net Hα emission and IR excess, a large intrinsic scatter is also observed between different sources, and therefore it is not trivial to account for this extra emission (Coté & Waters 1987; van Kerkwijk, Waters, & Marlborough 1995). Furthermore, the continuum level can be affected by the stellar rotation, especially when the star is rotating close to its critical velocity (Townsend, Owocki, & Howarth 2004). The assigned spectral type might not account fully for such deviation from the continuum level that would be observed in the case of a non-rapidly rotating star of the same spectral type. Nevertheless, because we are only interested in the synthetic continuum level as a check for the photometrically derived values, we neglect the contribution to the continuum level from the circumstellar region and any possible changes due to the stellar rotation. Taking the same approach as in equation (4) we can calculate a synthetic Hα luminosity using

$$L_{\mathrm{H}\alpha}^{\mathrm{S}} = 4\pi R_{\star}^{2} \mathcal{F}_{\star}^{\mathrm{S}} E_{\mathrm{H}\alpha}, \tag{5}$$

where $E_{\mathrm{H}\alpha}$ is the net Hα emission discussed in § 4.2. The $L_{\mathrm{H}\alpha}^{\mathrm{S}}$ values for all seven stars are listed in Table 6.

5. Discussion

5.1. The Hα Emission as a Tracer of the Circumstellar Disk

We begin by looking at the relationship between the Hα emission and the physical extent of the circumstellar region. Using the values for the Hα luminosity from Table 6 and the physical size of the major axis from Table 3, we construct a corresponding log-log plot of $L_{\mathrm{H}\alpha}$ versus D_{mj} in Figure 10. We obtain a Pearson correlation coefficient of 0.98 and thus a definite correlation between the parameters exists. Fitting a line to the data in the log-log plot yields a slope of 2.12±0.24 and a χ_{ν}^{2} of 0.75.

The above result suggests that the emission is proportional to the area of the Hα-emitting region independently of the different inclination angles at which these systems are viewed (although the range of possible inclination angles represented by our small sample of stars is not that large). If the circumstellar region is optically thin to Hα emission then this might simply mean that the *emission measure*[1] of the disk, which is proportional to the emitting volume, scales as the surface area of the emitting region. However, the study of energetics of Be star envelopes by Millar, Sigut, & Marlborough

[1]Because the Hα emission is created by recombinations, the total emission in the optically thin case is proportional to the volume integrated squared electron number density, i.e. $\int N_{\mathrm{e}}^{2} \mathrm{d}V$, which is also known as the emission measure (see, for example, Millar, Sigut, & Marlborough 2000).

(2000) shows that the Hα emission originating in the equatorial plane of the circumstellar disk, especially close to the central star (for $r < 15R_\star$), is optically thick. Because this is the same region that is responsible for the majority of the line emission, and if the disk has a constant surface brightness, then the Hα luminosity might be expected to be proportional to the effective surface area of the circumstellar disk.

If we assume that the circumstellar region is a geometrically thin axisymmetric disk, then the axial ratio, r, we have obtained from the elliptical Gaussian model can be used to estimate the inclination angle i between the direction perpendicular to the plane of the disk and the line of sight (i.e., $r \sim \cos i$). Because the effective area of a disk viewed at an angle i can be expressed as $A \cos i$ where A is the surface area, and if the Hα luminosity is proportional to the effective area, dividing $L_{\mathrm{H}\alpha}$ by r should remove any dependence on the inclination angle. Figure 11 shows the relationship between $L_{\mathrm{H}\alpha}/r$ and D_{mj} where again the correlation coefficient is high (0.96) and the best-fit line has a slope of 2.24±0.26 and χ^2_ν of 1.19. Based on this result we conclude that the Hα luminosity (corrected for the projection effect) is consistent with an optically thick emission from a geometrically thin disk of a relatively constant surface brightness.

Optically thick disks with no temperature gradients will have a constant surface brightness as a function of radius. Although actual disks will have a range of temperatures, assigning a constant temperature to the Hα-emitting region might be appropriate. This is because Millar & Marlborough (1999c), who, by considering the rates of energy gain and loss in the disks of four Be stars (including γ Cas, ψ Per, and β CMi), have shown that the disk temperature in the equatorial plane is fairly constant as a function of radial distance, especially in the regions close to the central star (i.e., where the majority of the Hα flux is expected to originate). Furthermore, our results suggest that the surface brightness in the Hα-emitting region is not only constant as a function of radial distance, but that it does not vary significantly for stars of different effective temperatures. This is somewhat surprising, considering that the disk models of Millar & Marlborough (1999c) for stars of different effective temperatures do not have the same temperature profiles as function of radial distance, although in the inner part of the disks ($< 10R_\star$) the temperature differences are not that large and are in the 3,000–5,000 K range (depending on the distance from the equatorial plane). It is also possible that because the Hα emission is optically thick in these inner regions (Millar, Sigut, & Marlborough 2000), the similar surface brightnesses for disks with slightly different temperatures is a result of similar conditions in the envelopes where the optical depth is roughly unity (i.e., where most of the radiation originates).

Lastly, we need to verify that the visible trend in Figure 10 (as well as Fig. 11) is not a result of the functional dependence of D_{mj} and $L_{\mathrm{H}\alpha}$ on the same determination of distance d, which by itself will tend to introduce correlation between the two parameters. To verify that the correlations are not caused by the dependence on d alone, we use the synthetic Hα

luminosities (recall § 4.3.2), which are measured with respect to the synthetic continuum levels and thus are independent of d, and we analyze the relationships between $L^{\rm S}_{{\rm H}\alpha}$ and $L^{\rm S}_{{\rm H}\alpha}/r$ versus $D_{\rm mj}$ in Figures 12 and 13, respectively. Because only the abscissa depends on the distance in this case, a trend can no longer be caused by the functional dependence on distance. These relations yield best-fit slopes of 1.98±0.33 and 2.28±0.38 (and correlation coefficients of 0.91 and 0.96), in complete agreement with our previously determined values. The χ^2_ν values for the relations based on the synthetic continuum levels are slightly larger (approximately twice as large) than before, but this might be solely related to the unaccounted systematic uncertainties associated with the estimated radii, as well as with the fact that the synthetic spectra do not account for the continuum emission from the circumstellar regions.

5.2. Disk Size and Stellar Properties

5.2.1. Size versus Spectral Type

The origin of the circumstellar regions around Be stars is still debated. One of the simpler tests is to search for a possible correlations between the size of the circumstellar region and the spectral type of the central star. Figure 14 illustrates the relationship between the physical extent of the major axis and the spectral type for the seven stars listed in Table 3. Within our small sample of stars, it appears that the size of the Hα-emitting region decreases toward later spectral type. This is also shown in Figure 15, which plots $D_{\rm mj}$ versus the effective temperature from Table 5. The visible correlation is not nearly as strong as the one found for the Hα emission and the size of the emitting region, but it still yields a correlation coefficient of 0.75 and a slope of 1.29±0.19. Unfortunately, the small number statistics make these results tentative, but with future observations of a larger set of stars, it will be possible to explore this relationship further.

If the apparent dependence of $D_{\rm mj}$ on the spectral type is real, it is possible that this is due to the tendency of hotter stars to have physically larger circumstellar regions, but equivalently this can also be attributed to a simple ionization effect. For example, Millar & Marlborough (1999a) investigated models of circumstellar regions of Be stars with a range of effective temperatures and concluded that in the case of the hot Be star γ Cas, the circumstellar envelope is almost completely ionized, in contrast to the cool Be stars (like β CMi), whose envelopes in and near the equatorial plane (where most of the emission normally originates) is mostly neutral (see also Millar & Marlborough 1998, 1999b). This suggests that the cooler Be stars might have smaller Hα-emitting regions due to the ionization-bounded conditions in their circumstellar regions.

5.2.2. Size versus Rotational Velocity

Another commonly examined relationship is the one between the size of the region and the rotational velocity. The connection between the two would be expected if rotation has a direct effect on the disk formation, as originally suggested by Struve (1931). In Table 7 we list the $v \sin i$ values from Slettebak (1982), the estimated[2] rotational velocities ($v_{\rm est}$), along with the critical velocities from Porter (1996). We find no correlation between the physical extent of the Hα-emitting region and the observed $v \sin i$ value. This is in agreement with previous studies that concluded that there is no correlation between the strength of the Hα emission and the $v \sin i$ value.

Because we derive an inclination angle i from the apparent ellipticity of the Hα-emitting disk, our estimates on the rotational velocities of Be stars are quite independent of the estimates that are obtained for systems that are thought to be viewed edge-on (i.e., using Be-shell stars). Therefore our estimate on the average rotational velocity, expressed as a fraction of $v_{\rm crit}$, should be independent of similar estimates obtained from observations of Be-shell stars. In Table 7 we list the values of the ratio of $v_{\rm est}$ to $v_{\rm crit}$ for all stars, including 48 Per for which only a lower limit can be obtained (see also Fig. 16). We obtain a weighted average (excluding 48 Per) of 0.64±0.14 for $v_{\rm est}/v_{\rm crit}$, which is in excellent agreement with the work of Porter (1996), who concluded that the distribution of the rotational velocities is sharply peaked at $\sim$0.7$v_{\rm crit}$.

Assuming that the $v \sin i$ values obtained from spectral lines are not underestimated (for example due to the equatorial gravity darkening caused by rapid rotation), the above result suggests that Be stars are rotating well below their critical limits. On the other hand, if the $v \sin i$ values are systematically underestimated by tens of percent (as suggested by Townsend, Owocki, & Howarth 2004), then it is still possible that these stars have near-critical rotation rates. A much more direct method for determining the rotational velocity of stars is the observation of the rotationally induced distortion of the stellar photosphere by long-baseline interferometry. In fact, the first result suggesting a near-critical rotation in the case of one Be star already exists (Domiciano de Souza et al. 2003). It is anticipated that with the advent of optical interferometric observations at baselines of hundreds of meters (such as those of the NPOI), further observational constraints on the stellar rotation and its role in Be disk formation will be possible.

---

[2]The rotational velocity is estimated by assuming that the circumstellar envelope is a thin axisymmetric disk that is aligned with the stellar equator, in which case the axial ratio, r, can be used to estimate i.

6. Conclusions

Our analysis of the relationship between the net Hα emission and the physical extent of the emitting circumstellar region produced a clear correlation between the two properties for the first time. The functional dependence between the parameters suggests that the emission is directly proportional to the effective surface area of the emitting disk. These results are consistent with an optically thick Hα emission from a geometrically thin circumstellar disk. We do not detect any significant degree of correlation between the size of the circumstellar region and the stellar rotation rate, although the data suggest that hotter Be stars might have more extended Hα-emitting regions. Extending our analysis to a larger sample of stars will verify if this is indeed a general property of classical Be stars.

Because the formation and the subsequent evolution of the circumstellar disks around Be stars are still the long-standing puzzles associated with these stars, the interferometric investigations by long-baseline interferometers will play a crucial role in our understanding of these objects. Already in the near-term it should be possible to detect small-scale structures within the circumstellar disks and investigate the characteristics of the inner disk regions, thereby putting specific constraints on disk formation theories. Imaging small-scale structures, such as one-armed density waves or spiral structures, will yield direct information about the instabilities in the disks, possibly related in some cases to unseen binary companions. Also, combining spectroscopic and interferometric observations, especially in the context of mass ejection episodes (which in some cases might be predicted based on spectroscopy) will play a crucial role in our understanding of the mass-feeding mechanisms, and the subsequent evolution of the material in the disk. Lastly, the direct detection of the deviation from circular symmetry of the stellar surface, due to rapid rotation, will help establish the connection between the stellar rotation and the disk formation, independently of (or in conjunction with) spectroscopic studies.

The multi-spectral and the Hα-filtering capabilities of the NPOI make it an optimal instrument to address the above described issues. We are currently setting up the NPOI for observations at baselines of up to 100 m, which will allow us to study the spatial properties of the Hα-emitting regions of Be stars in ways not possible before. Such studies have the potential of not only contributing to our understanding of these interesting objects, but they might also make a significant contribution to other branches of stellar astrophysics. For example, the investigation of disk formation mechanism(s) will contribute to our understanding of asymmetric mass-loss processes including stellar angular momentum distribution (especially in the context of rapidly rotating stars). The apparent outflow of the material in the circumstellar disk and its possible eventual dispersal, can be used as a test ground for examining theories related to angular momentum transfer in outflowing disks.

The Navy Prototype Optical Interferometer is a joint project of the Naval Research Laboratory and the US Naval Observatory, in cooperation with Lowell Observatory, and is funded by the Office of Naval Research and the Oceanographer of the Navy. We would like to thank Wes Lockwood for accommodating our observing requests and for providing us with the echelle spectra from the Lowell Observatory's Solar-Stellar Spectrograph. We thank David Mozurkewich and the anonymous referee for useful comments on how to improve the manuscript. C.T. acknowledges that this work was performed in part as a Ph.D. research at the University of Toronto under funding from the Government of Ontario Graduate Scholarship in Science and Technology and Walter C. Sumner Fellowship, as well as in part while being employed by the NVI, Inc. at the US Naval Observatory under contract N0060001C0339. Part of this work was also performed under a contract with the Jet Propulsion Laboratory (JPL) funded by NASA through the Michelson Fellowship Program. JPL is managed for NASA by the California Institute of Technology. This research has made use of the SIMBAD literature database, operated at CDS, Strasbourg, France.

REFERENCES

Andrillat, Y. & Fehrenbach, C. 1982, A&AS, 48, 93

Armstrong, J. T., Mozurkewich, D., Rickard, L. J., Hutter, D. J., Benson, J. A., Bowers, P. F., Elias II, N. M., Hummel, C. A., Johnston, K. J., Buscher, D. F., Clark III, J. H., Ha, L., Ling, L.-C., White, N. M., & Simon, R. S. 1998, ApJ, 496, 550

Banerjee, D. P. K., Rawat, S. D., & Janardhan, P. 2000, A&AS, 147, 229

Beeckmans, F. & Hubert-Delplace, A. M. 1980, A&A, 86, 72

Böhm-Vitense, E. 1981, ARA&A, 19, 295

Coté, J., & Waters, L. B. F. M. 1987, A&A, 176, 93

Domiciano de Souza, A., Kervella, P., Jankov, S., Abe, L., Vakili, F., di Folco, E., & Paresce, F. 2003, A&A, 407, L47

ESA 1997, The Hipparcos and Tycho Catalogues (ESA SP-1200) (Noordwijk:ESA)

FitzGerald, M. P. 1970, A&A, 4, 234

Hall, J. C., Fulton, E. E., Huenemoerder, D. P., Welty, A. D., & Neff, J. E. 1994, PASP, 106, 315

Hanuschik, R. W., Hummel, W., Sutorius, E., Dietle, O., & Thimm, G. 1996, A&AS, 116, 309

Hoffleit, D. & Jaschek, C. 1982, The Bright Star Catalogue, New Haven: Yale University Observatory (4th edition)

Hummel, C.A., Mozurkewich, D., Armstrong, J.T., Hajian, A.R., Elias II, N.M., & Hutter, D.J. 1998, AJ, 116, 2536

Hummel, W. & Vrancken, M. 1995, A&A, 302, 751

Johnson, H. L. 1966, ARA&A, 4, 193

Johnson, H. L., Iriarte, B., Mitchell, R. I., & Wisniewski, W. Z. 1966, Communications of the Lunar and Planetary Laboratory, 4, 99

Kurucz, R. L. 1993, CD-ROM 13, Atlas9 Stellar Atmosphere Programs and 2 km/s Grid (Cambridge: SAO)

Millar, C. E. & Marlborough, J. M. 1998, ApJ, 494, 715

Millar, C. E. & Marlborough, J. M. 1999a, ApJ, 516, 276

Millar, C. E. & Marlborough, J. M. 1999b, ApJ, 516, 280

Millar, C. E. & Marlborough, J. M. 1999c, ApJ, 526, 400

Millar, C. E., Sigut, T. A. A., & Marlborough, J. M. 2000, MNRAS, 312, 465

Mourard, D., Bosc, I., Labeyrie, A., Koechlin, L., & Saha, S. 1989, Nature, 342, 520

Porter, J. M. 1996, MNRAS, 280, L31

Porter, J. M., & Rivinius, T. 2003, PASP, 115, 1153

Quirrenbach, A., Hummel, C. A., Buscher, D. F., Armstrong, J. T., Mozurkewich, D., & Elias, N. M. 1993, ApJ, 416, L25

Quirrenbach, A., Buscher, D. F., Mozurkewich, D., Hummel, C. A., & Armstrong, J. T. 1994, A&A, 283, L13

Quirrenbach, A., Bjorkman, K. S., Bjorkman, J. E., Hummel, C. A., Buscher, D. F., Armstrong, J. T., Mozurkewich, D., Elias II, N. M., & Babler, B. L. 1997, ApJ, 479, 477

Schild, R. E. 1978, ApJS, 37, 77

Schild, R. E. 1983, A&A, 120, 223

Schultz, G. V. & Wiemer, W. 1975, A&A, 43, 133

Shao, M., & Staelin, D.H. 1980, Appl. Opt., 19, 1519

Shao, M., Colavita, M., Staelin, D. H., Johnston, K. J., Simon, R. S., Hughes, J. A., & Hershey, J. L. 1987, AJ, 93, 1280

Shao, M., Colavita, M. M., Hines, B. E., Staelin, D. H., & Hutter, D. J. 1988, A&A, 193, 357

Slettebak, A. 1982, ApJS, 50, 55

Slettebak, A., Collins, G. W., & Truax, R. 1992, ApJS, 81, 335

Stee, P., de Araujo, F. X., Vakili, F., Mourard, D., Arnold, L., Bonneau, D., Morand, F., & Tallon-Bosc, I. 1995, A&A, 300, 219

Struve, O. 1931, ApJ, 73, 94

Thom, C., Granes, P., & Vakili, F. 1986, A&A, 165, L13

Townsend, R. H. D., Owocki, S. P., & Howarth, I. D. 2004, MNRAS, 350, 189

Tycner, C., Hajian, A. R., Mozurkewich, D., Armstrong, J. T., Benson, J. A., Gilbreath, G. C., Hutter, D. J., Pauls, T. A., & Lester, J. B. 2003, AJ, 125, 3378

Tycner, C., Hajian, A. R., Armstrong, J. T., Benson, J. A., Gilbreath, G. C., Hutter, D. J., Lester, J. B., Mozurkewich, D., & Pauls, T. A. 2004, AJ, 127, 1194

Underhill, A. B., Divan, L., Prevot-Burnichon, M.-L., & Doazan, V. 1979, MNRAS, 189, 601

van Kerkwijk, M. H., Waters, L. B. F. M., & Marlborough, J. M. 1995, A&A, 300, 259

This preprint was prepared with the AAS LaTeX macros v5.2.

Table 1: Observing Log for η Tauri and β Canis Minoris

Date	η Tau # of scans	β CMi # of scans
1997 Oct 15	5	...
1997 Nov 6	11	4
1997 Nov 7	10	2
1997 Nov 8	...	3
1997 Nov 25	6	...
1997 Dec 5	3	...
1997 Dec 6	3	...
1998 Mar 22	...	4
1998 Oct 7	5	...
1998 Oct 11	8	...
1998 Oct 12	3	...
1998 Nov 25	4	3
1998 Dec 11	2	...
1998 Dec 12	5	...
1998 Dec 24	18	...
1999 Feb 27	2	2
1999 Feb 28	3	...
1999 Mar 1	4	...
1999 Mar 4	2	...
1999 Mar 20	3	...
1999 Mar 25	3	...
1999 Apr 10	...	2
Total	100	20

Table 2: Best-Fit Model Parameters for η Tauri and β Canis Minoris

	$\theta_{\rm mj}$ (mas)	r	ϕ (deg)	$c_{\rm p}$	χ^2_ν
η Tau	1.94 ± 0.12	1	...	0.895 ± 0.010	1.03
	2.08 ± 0.18	0.753 ± 0.053	44.6 ± 9.4	0.893 ± 0.015	0.88
β CMi	2.02 ± 0.28	1	...	0.904 ± 0.019	0.62
	2.13 ± 0.50	0.69 ± 0.15	40 ± 30	0.874 ± 0.069	0.54

Table 3: The Circumstellar Regions of Be Stars

HD	Star	Spectral Type	π (mas)	d (pc)	$\theta_{\rm mj}$ (mas)	r	$D_{\rm mj}$ (10^9 m)
(1)	(2)	(3)	(4)	(5)	(6)	(7)	(8)
5394	γ Cas	B0 IVe	5.32 ± 0.56	188^{+22}_{-18}	3.67±0.09	0.79±0.03	103^{+13}_{-10}
23630	η Tau	B7 IIIe	8.87 ± 0.99	113^{+14}_{-11}	2.08±0.18	0.75±0.05	$35.1^{+5.4}_{-4.7}$
37202	ζ Tau	B4 IIIpe	7.82 ± 1.02	128^{+19}_{-15}	3.14±0.21	0.31±0.07	$60.1^{+9.9}_{-8.0}$
58715	β CMi	B8 Ve	19.2 ± 0.85	$52.2^{+2.4}_{-2.2}$	2.13±0.50	0.69±0.15	$16.6^{+4.0}_{-4.0}$
10516	ϕ Per	B2 Vpe	4.55 ± 0.75	220^{+43}_{-31}	2.67±0.20	0.46±0.04	87.8^{+19}_{-14}
22192	ψ Per	B5 Ve	4.66 ± 0.73	215^{+40}_{-29}	3.26±0.23	0.47±0.11	105^{+21}_{-16}
25940	48 Per	B3 Ve	5.89 ± 0.72	170^{+24}_{-19}	2.77±0.56	0.89±0.13	70.4^{+17}_{-16}

Note.— Column 3: spectral type from the BSC. Column 4: parallax from the *Hipparcos* catalogue (ESA 1997). Column 5: distance to the source. Column 6: the angular diameter of the major axis of the elliptical Gaussian model representing the Hα-emitting envelope. Column 7: axial ratio of the elliptical Gaussian model. Column 8: $\theta_{\rm mj}$ in physical units.

Table 4: Photometric Data for Be Stars

Star	V	$B-V$	$(B-V)_0$	$E(B-V)$	$V-R$	$E(V-R)$	R_0
(1)	(2)	(3)	(4)	(5)	(6)	(7)	(8)
γ Cas	2.47	−0.15	−0.30	0.07	0.07	0.06	2.24
η Tau	2.87	−0.09	−0.12	0.03*	0.03	0.02	2.77
ζ Tau	3.00	−0.19	−0.18	0.05	−0.03	0.04	2.91
β CMi	2.90	−0.09	−0.11	0.02*	−0.01	0.02	2.86
ϕ Per	4.07	−0.04	−0.24	0.11	0.16	0.09	3.65
ψ Per	4.23	−0.06	−0.16	0.10	0.10	0.08	3.89
48 Per	4.04	−0.03	−0.20	0.17	0.12	0.13	3.52

Note.— Columns 2 and 3: The apparent V magnitude and $B-V$ color from the BSC. Column 4: Intrinsic $(B-V)_0$ color based on the spectral type (FitzGerald 1970). Column 5: $E(B-V)$ based on the absorption bump at 2200 Å (Beeckmans & Hubert-Delplace 1980), except where denoted by * for values obtained from the estimated $(B-V)_0$ color. Column 6: $V-R$ colors from Johnson et al. (1966). Column 7: $E(V-R)$ derived from $E(V-R)/E(B-V) = 0.78 \pm 0.02$ (Schultz & Wiemer 1975). Column 8: Absolute R magnitude corrected for interstellar extinction.

Table 5: Estimated Stellar Properties

Star	$f_\star$ (10^{-12} W/m^2/nm)	$4\pi d^2 f_\star$ (10^{25} W/nm)	$T_{\rm eff}$ (K) ±5%	$R_\star$ ($R_\odot$)	$4\pi R_\star^2 \mathcal{F}_\star^{\rm S}$ (10^{25} W/nm)
γ Cas .	2.71	114^{+27}_{-22}	31,000	8±2	97 ± 50
η Tau .	1.65	$25.2^{+6.3}_{-5.1}$	12,400	5±1	8.60 ± 3.5
ζ Tau .	1.45	$28.4^{+8.5}_{-6.5}$	16,400	6±1	18.8 ± 6.6
β CMi	1.52	$4.95^{+0.46}_{-0.42}$	12,000	3.6±0.3	4.14 ± 0.81
ϕ Per ..	0.735	42.5^{+17}_{-12}	21,500	6.0±0.2	28.5 ± 3.4
ψ Per .	0.587	$32.4^{+12}_{-8.8}$	15,400	4.7±0.3	10.5 ± 1.7
48 Per .	0.830	$28.6^{+8.0}_{-6.2}$	19,000	5.1±0.1	16.9 ± 1.8

Note.— $f_\star$ is the physical flux (surface brightness) and $4\pi d^2 f_\star$ (where d is the distance to the source from Table 3) is the corresponding total radiation in the Hα region based on photometric data from Table 4. The effective temperature ($T_{\rm eff}$) and the stellar radius ($R_\star$) are based on the spectral type and tabulations of Böhm-Vitense (1981) and Underhill et al. (1979), respectively.

Table 6: The Hα Emission of Be Stars

Star	$W_{\rm H\alpha}$ (nm)	$E_{\rm H\alpha}$ (nm)	$L_{\rm H\alpha}$ (10^{25} W)	$L_{\rm H\alpha}^{\rm S}$ (10^{25} W)
γ Cas	-2.25 ± 0.11	-2.51 ± 0.12	287^{+69}_{-56}	250 ± 130
η Tau	-0.426 ± 0.021	-1.02 ± 0.03	$25.6^{+6.5}_{-5.2}$	8.7 ± 3.6
ζ Tau	-2.06 ± 0.10	-2.55 ± 0.11	72.2^{+22}_{-17}	48 ± 17
β CMi	-0.334 ± 0.017	-0.942 ± 0.026	$4.66^{+0.45}_{-0.42}$	3.90 ± 0.77
ϕ Per	-3.50 ± 0.18	-3.87 ± 0.18	165^{+65}_{-47}	110 ± 14
ψ Per	-3.37 ± 0.17	-3.89 ± 0.17	126^{+47}_{-35}	40.8 ± 6.9
48 Per	-2.23 ± 0.11	-2.68 ± 0.12	77^{+22}_{-17}	45.3 ± 5.2

Note.— The Hα equivalent widths ($W_{\rm H\alpha}$) are taken from a number of different sources (see § 3) and their uncertainties are assumed to be at 5% level to account for observational errors as well as possible intrinsic variability.

Table 7: Rotational Velocities of Be Stars

Star	$v \sin i$ (km s^{-1})	$v_{\rm est}$ (km s^{-1})	$v_{\rm crit}$ (km s^{-1})	$v_{\rm est}/v_{\rm crit}$
γ Cas	230±23	375±40	538±54	0.70±0.10
η Tau	140±14	212±28	406±41	0.53±0.09
ζ Tau	220±22	231±28	441±44	0.52±0.08
β CMi	245±25	338±75	397±40	0.85±0.21
ϕ Per	400±40	450±46	477±48	0.94±0.14
ψ Per	280±28	317±38	428±43	0.74±0.12
48 Per	200±20	$\gtrsim 308$	458±46	$\gtrsim 0.67$

Note.— The $v \sin i$ values are from Slettebak (1982), and $v_{\rm crit}$ values are from Porter (1996).

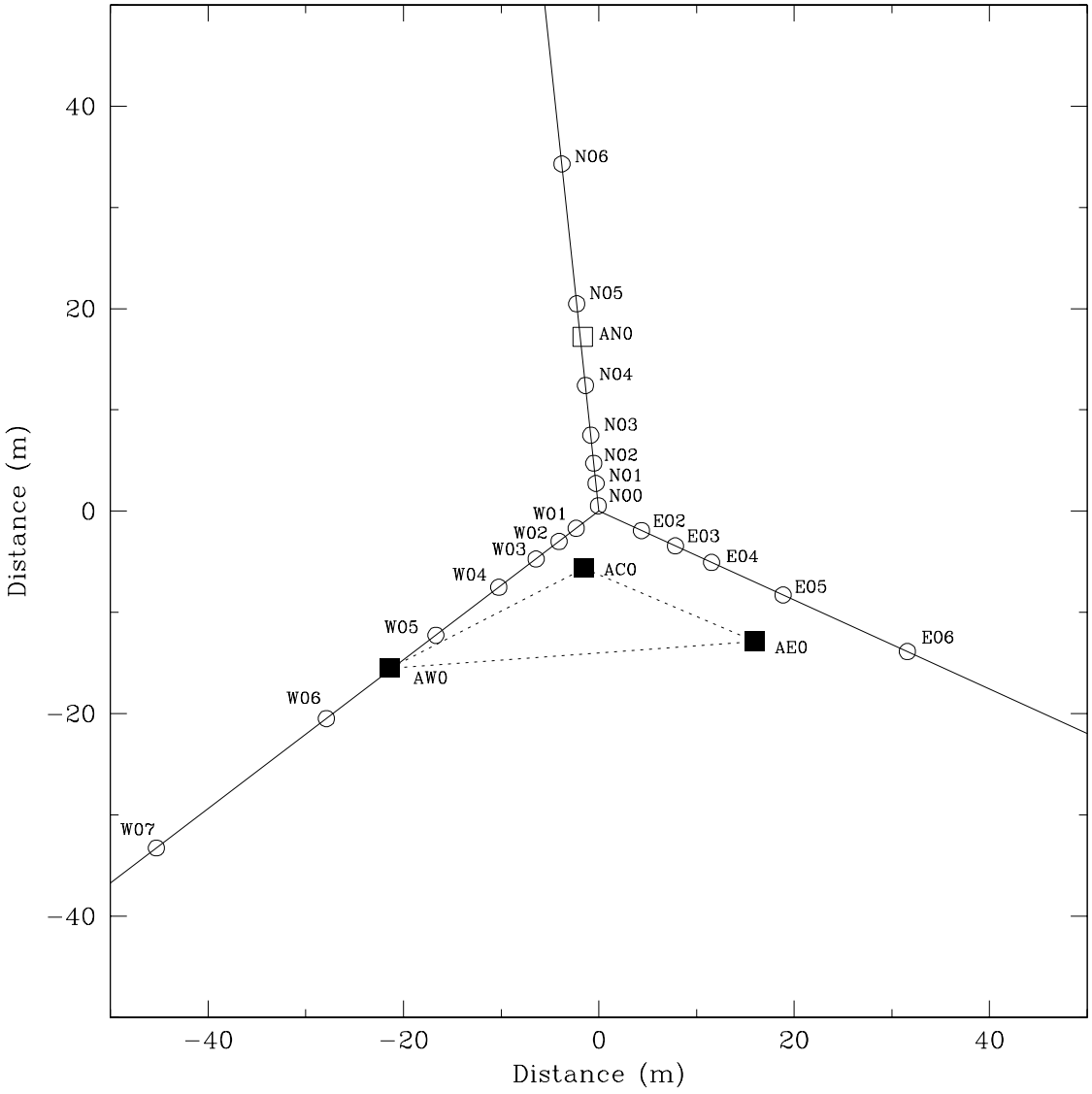

Fig. 1.— A schematic of the inner region of the NPOI array. Both the imaging (*circles*) and the astrometric (*squares*) stations are shown. The three astrometric stations used in the observations presented in this paper are shown with filled squares. The resulting baselines (*dotted lines*) have lengths of 18.9 (AC0–AE0), 22.2 (AW0-AC0), and 37.5 m (AW0–AE0) and are at azimuths of $-67\overset{\circ}{.}5$, $63\overset{\circ}{.}6$, and $86\overset{\circ}{.}0$, respectively.

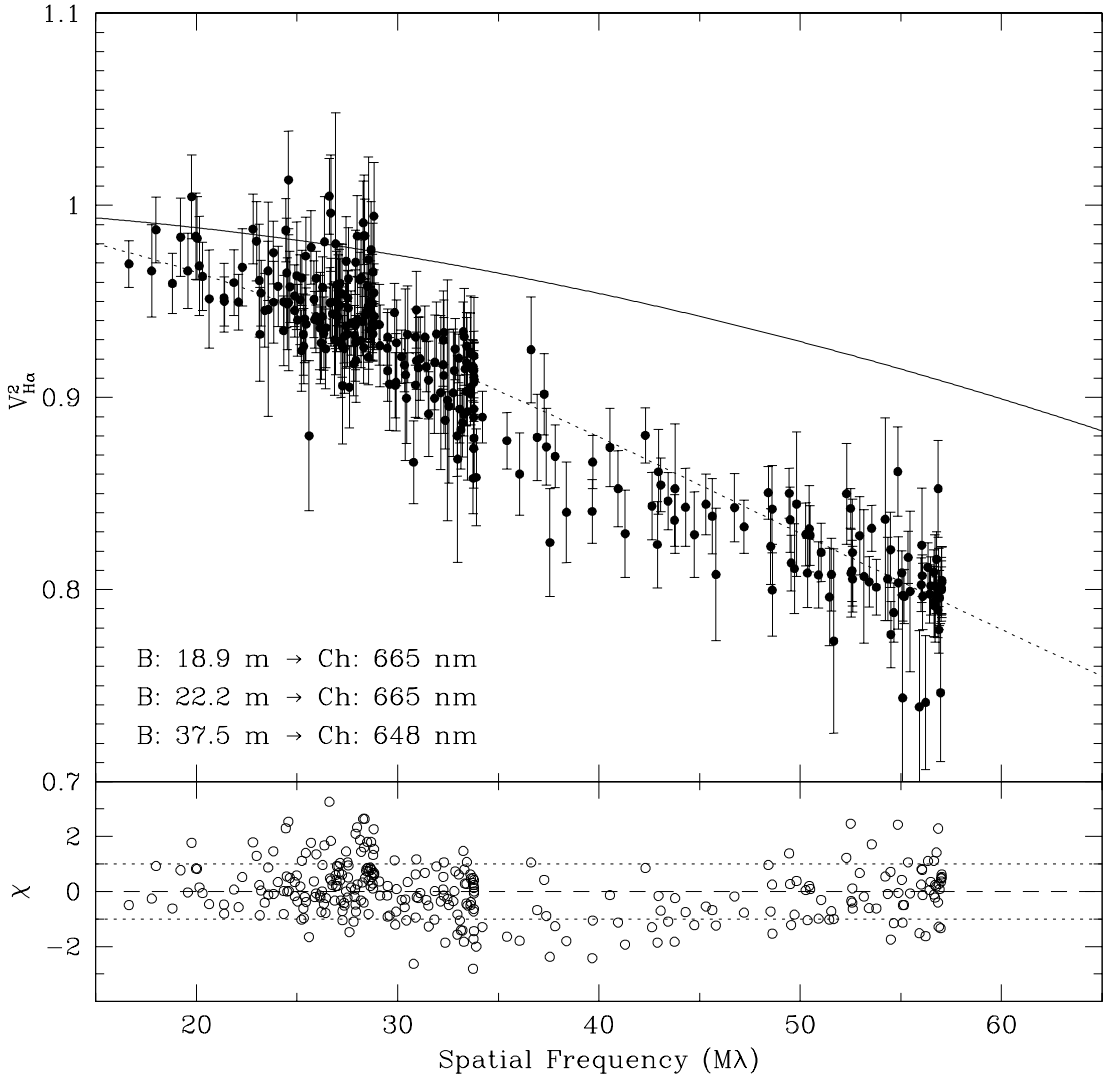

Fig. 2.— Calibrated squared visibilities of η Tau from the spectral channels that contain the Hα emission (i.e., 665 nm channel for the 18.9 and 22.2 m baselines, and 648 nm channel for the 37.5 m baseline). The uniform disk model representing the stellar photospheric disk (*solid-line*) and the best-fit circularly symmetric Gaussian model (*dotted-line*) are also shown. The normalized residuals for the circularly symmetric Gaussian are shown in the lower panel.

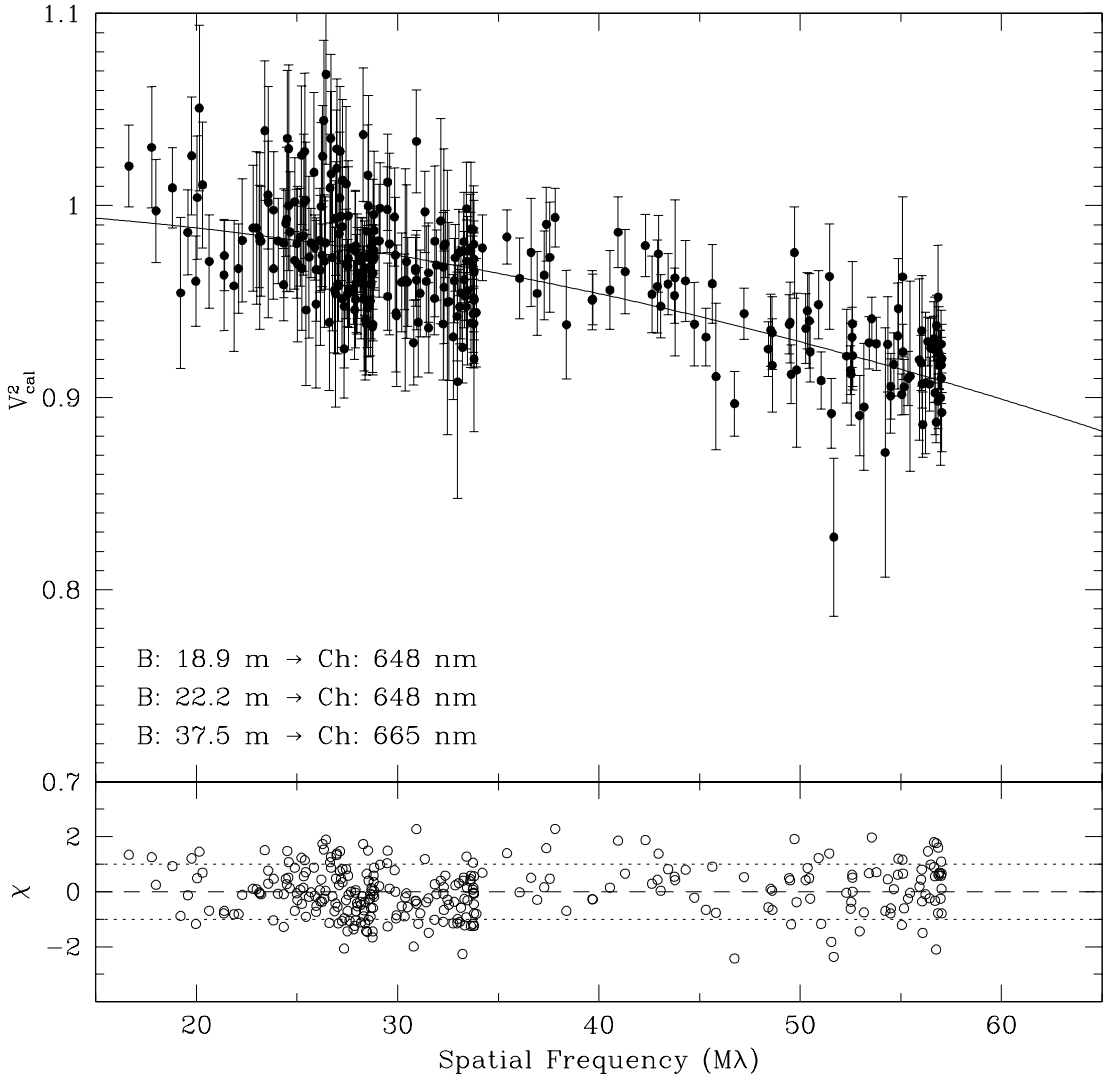

Fig. 3.— Same as Fig. 2 but with the choice of the spectral channels reversed (i.e., the 648 nm channel was used for the two shortest baselines and the 665 nm channel for the longest baseline). The residuals in the lower panel are calculated with respect to the uniform disk model representing the stellar photosphere.

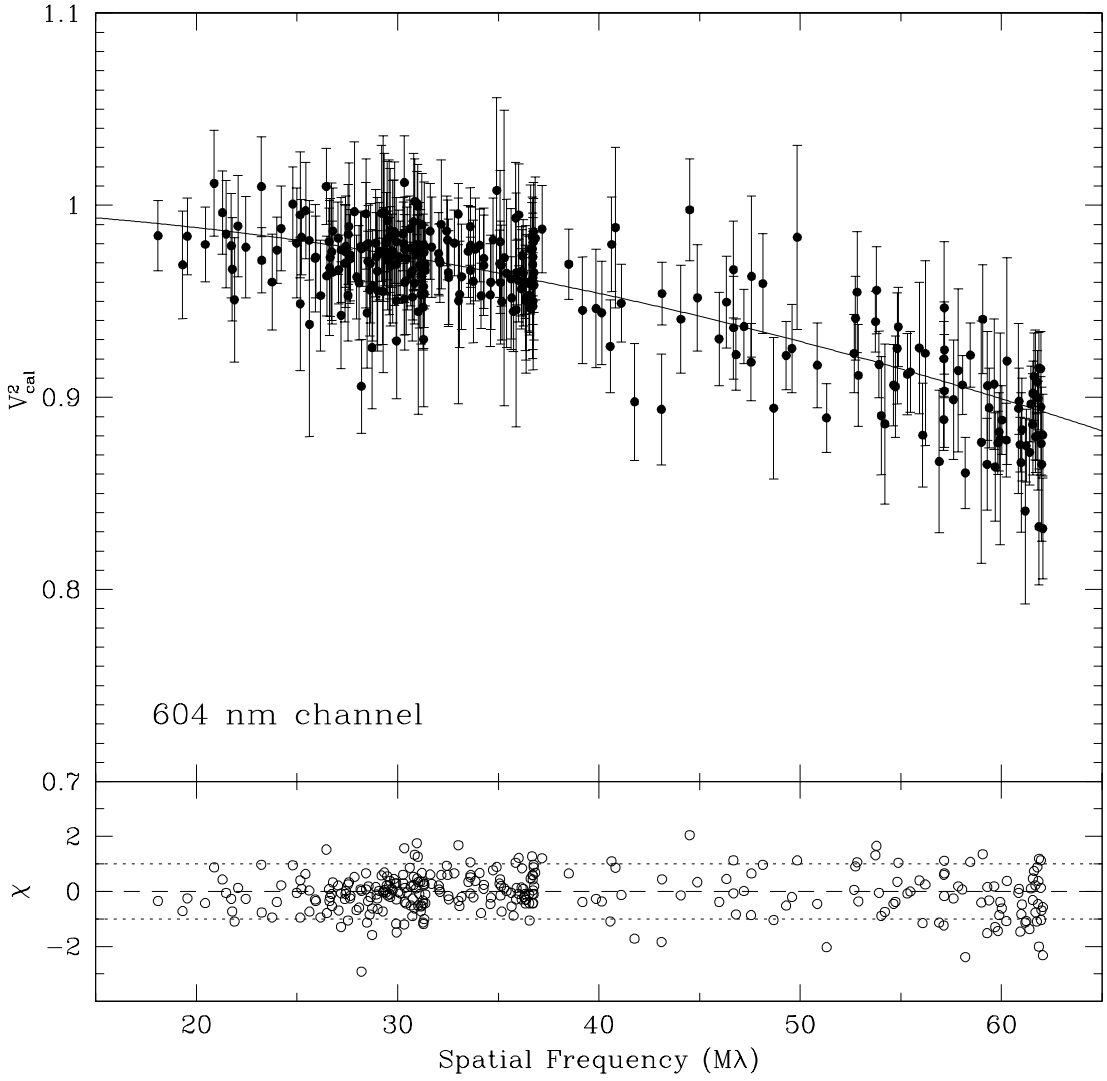

Fig. 4.— Calibrated squared visibilities of η Tau from the continuum channel at 604 nm.

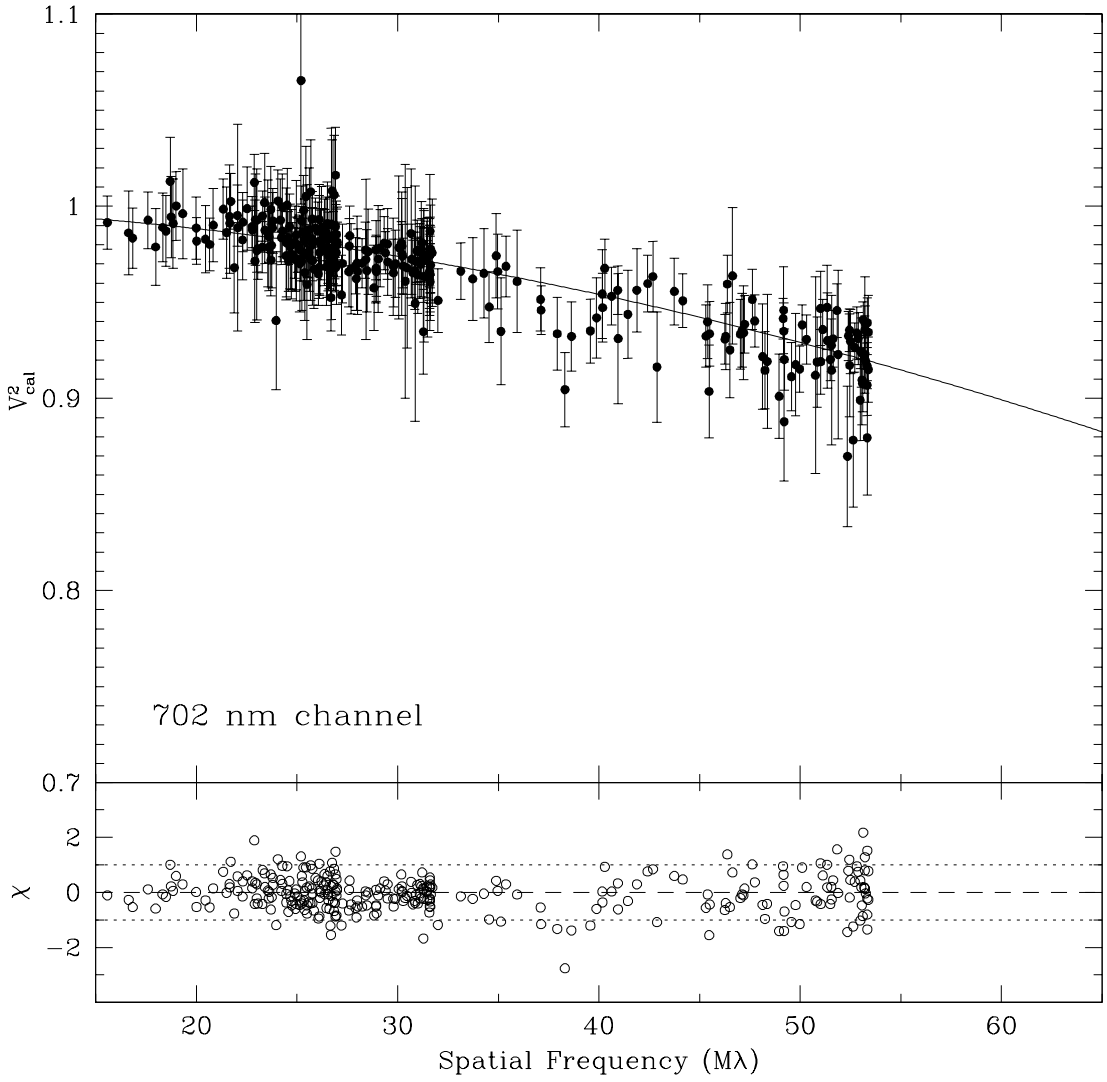

Fig. 5.— Same as Fig. 4 but for the continuum channel at 702 nm.

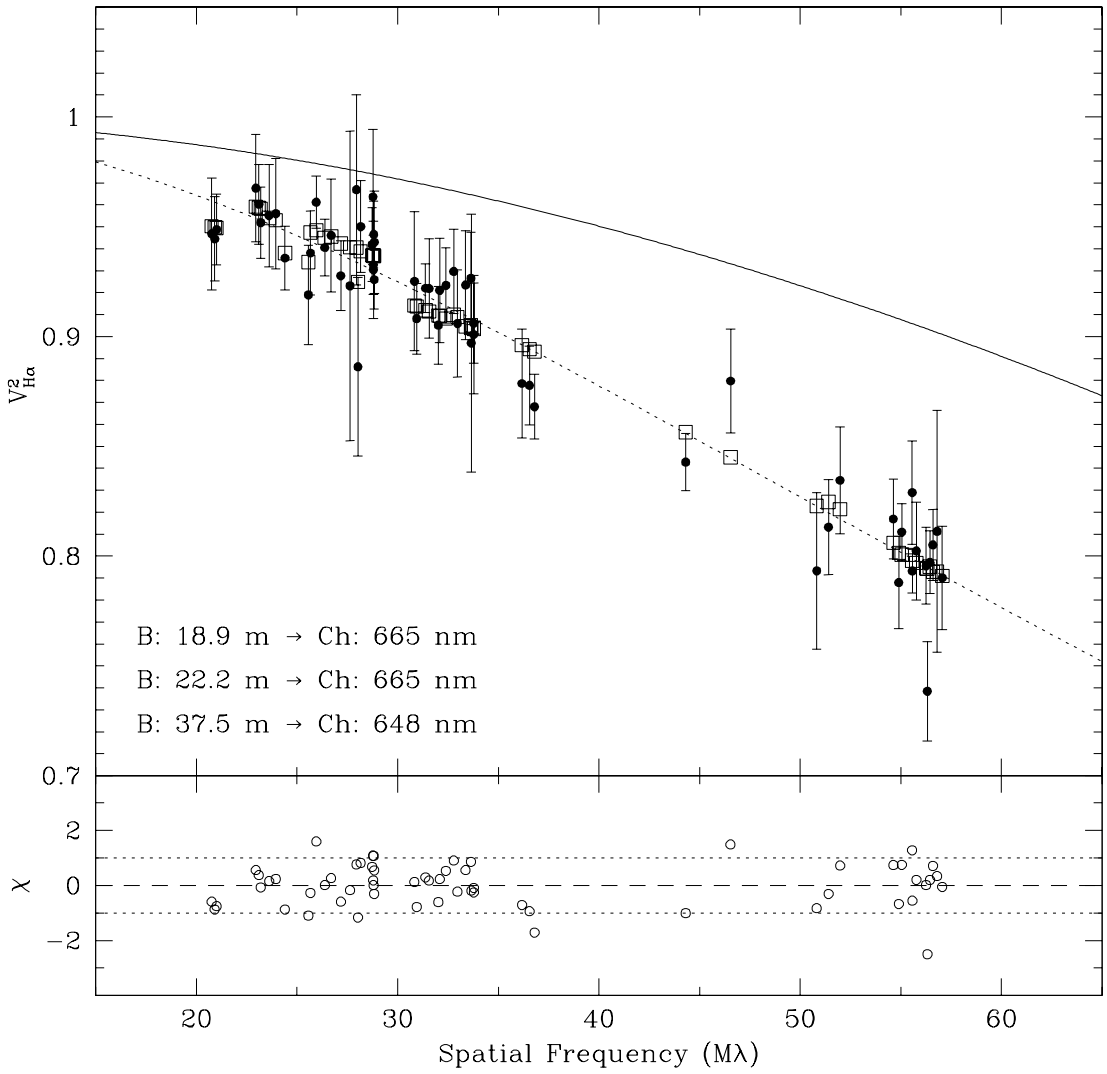

Fig. 6.— Calibrated squared visibilities of β CMi from the spectral channels that contain the Hα emission (i.e., 665 nm channel for the 18.9 and 22.2 m baselines, and 648 nm channel for the 37.5 m baseline). The uniform disk model representing the stellar photospheric disk (*solid line*) and the best-fit circularly symmetric (*dotted line*) and elliptical (*squares*) Gaussian models are also shown. The normalized residuals for the circularly symmetric Gaussian model are shown in the lower panel.

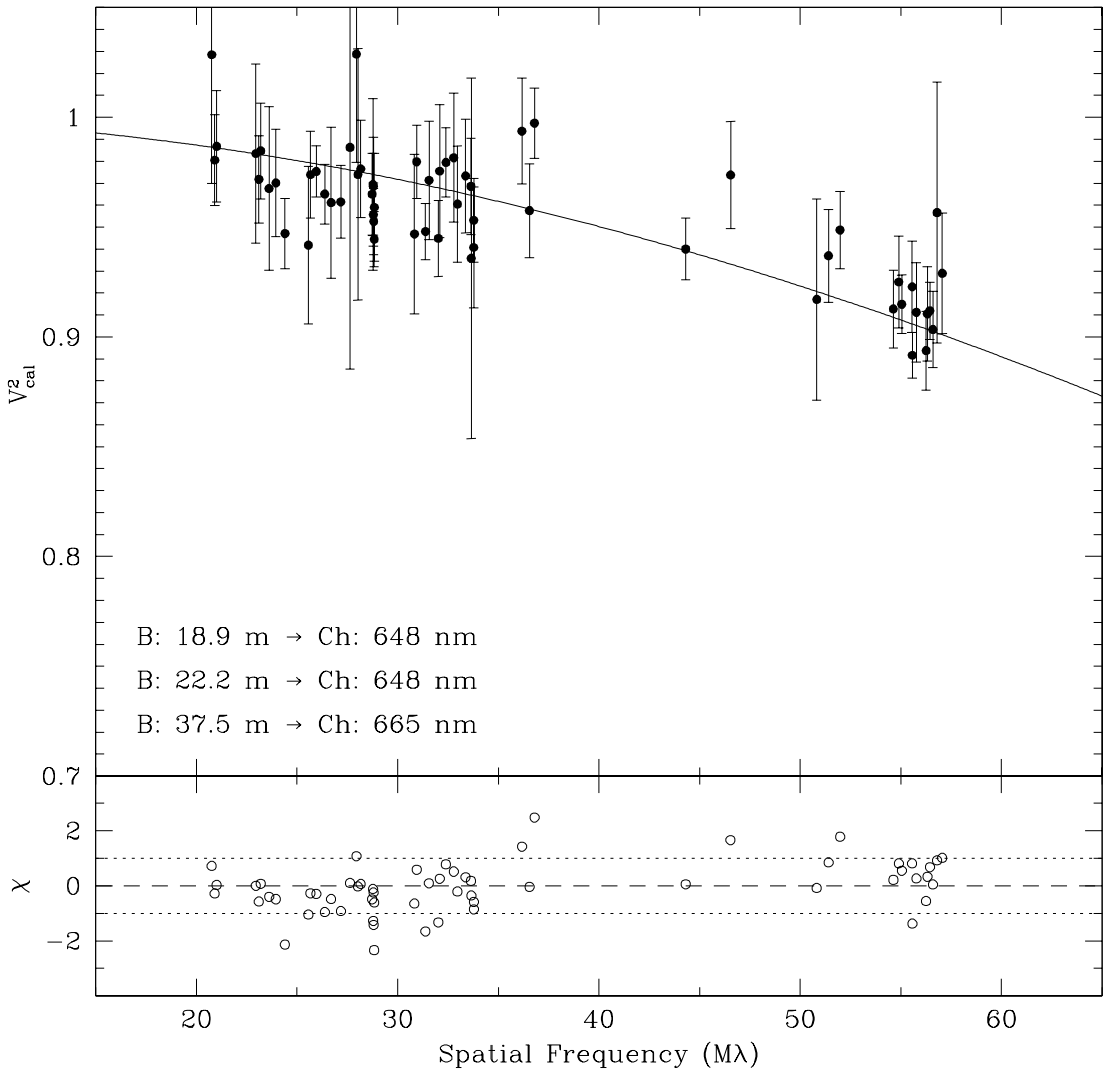

Fig. 7.— Same as Fig. 6, but with the choice of the spectral channels reversed. The residuals in the lower panel are calculated with respect to the uniform disk model representing the stellar photosphere.

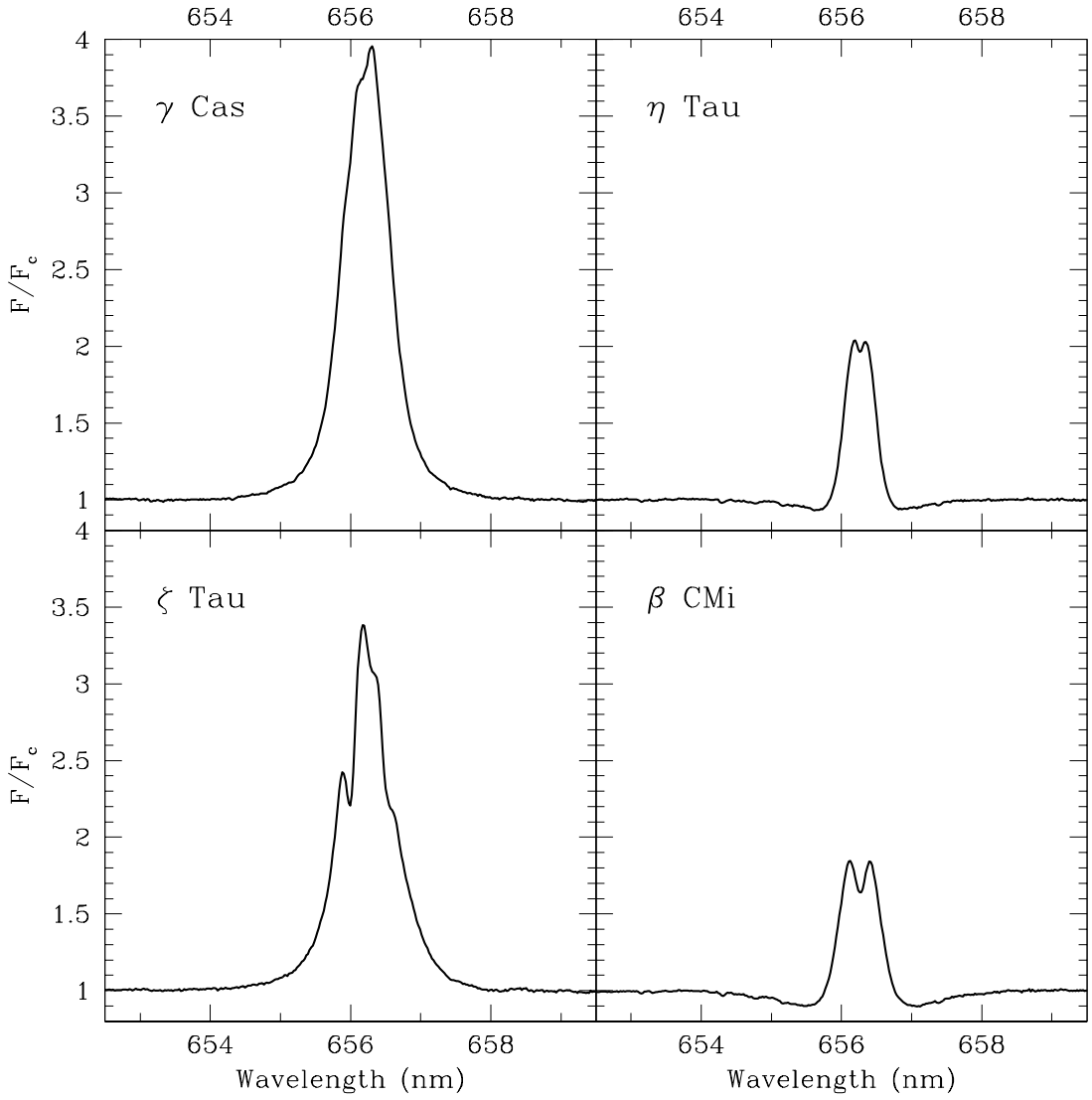

Fig. 8.— The Hα profiles of the four Be stars obtained with the Solar-Stellar Spectrograph. Each panel shows only a fraction of the 648–660 nm spectral region covered by the echelle order that contained the Hα line.

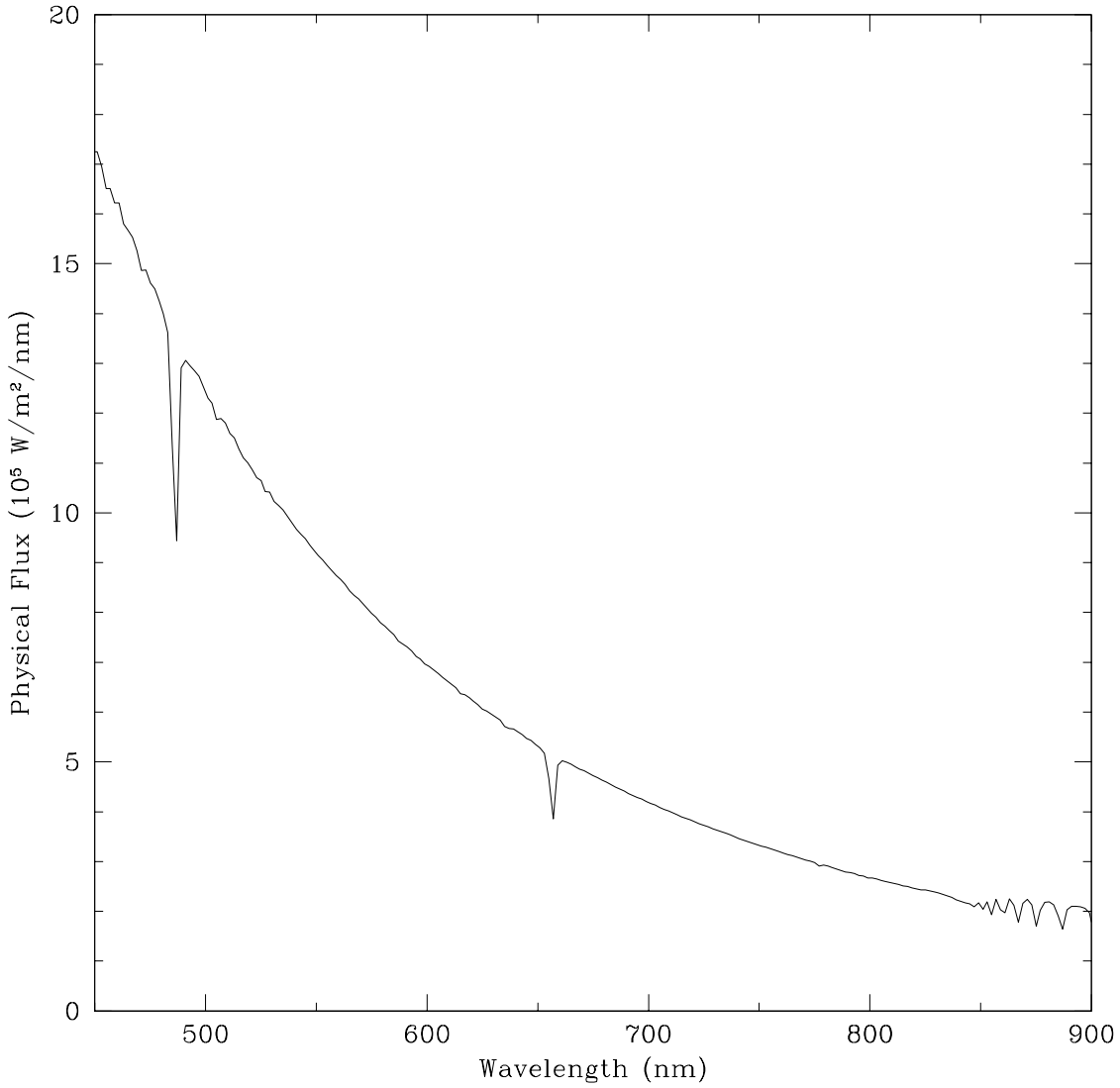

Fig. 9.— Synthetic energy distribution for $T_{\rm eff} = 12000$ K and $\log g = 4.0$.

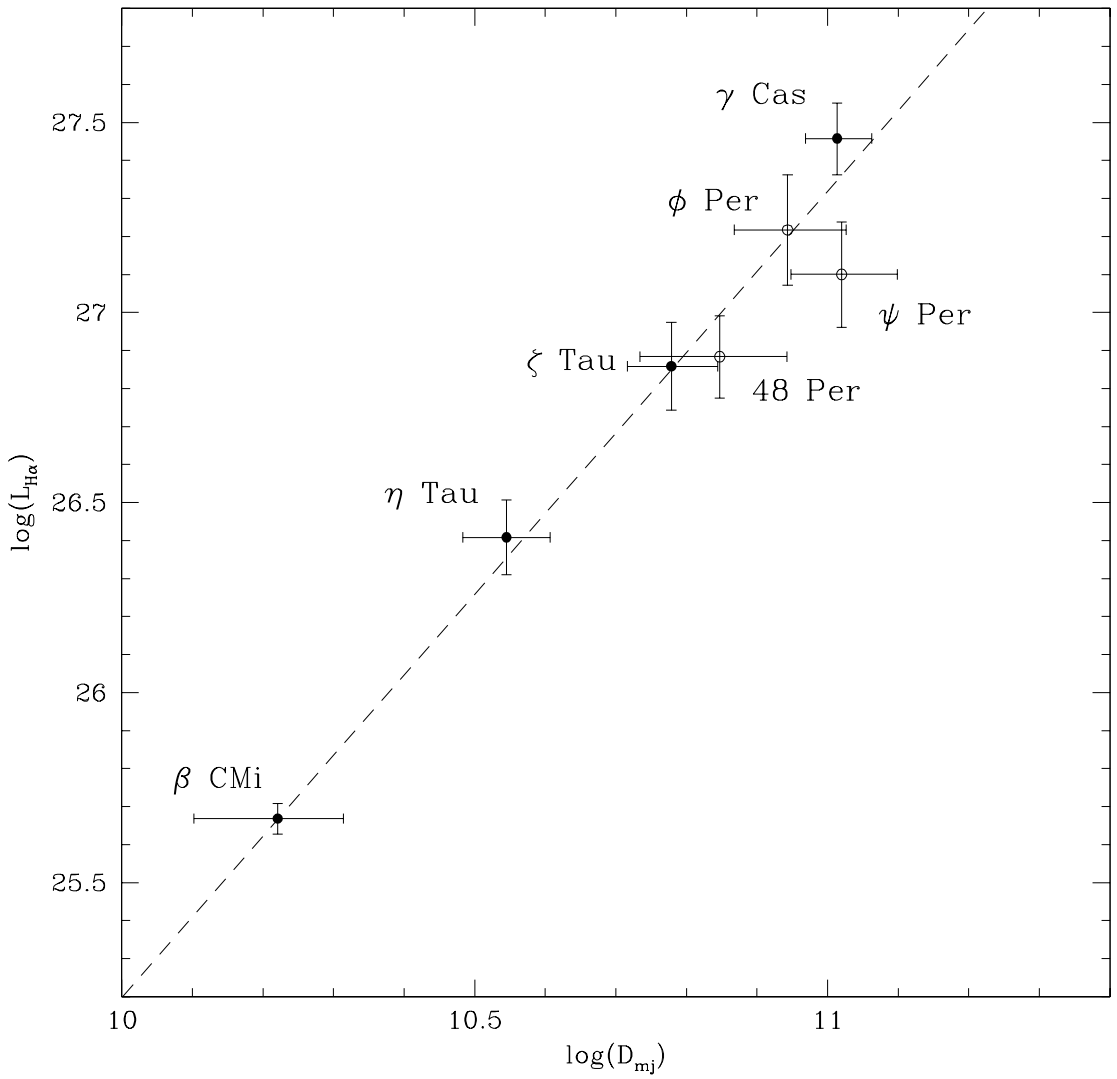

Fig. 10.— The Hα luminosity as a function of the size of the major axis of the disk. The circumstellar envelopes that have been resolved by the Mark III interferometer (Quirrenbach et al. 1997) are marked with *open circles*. A linear fit in the log-log plot produces a best-fit slope of 2.12±0.24 (*dashed line*).

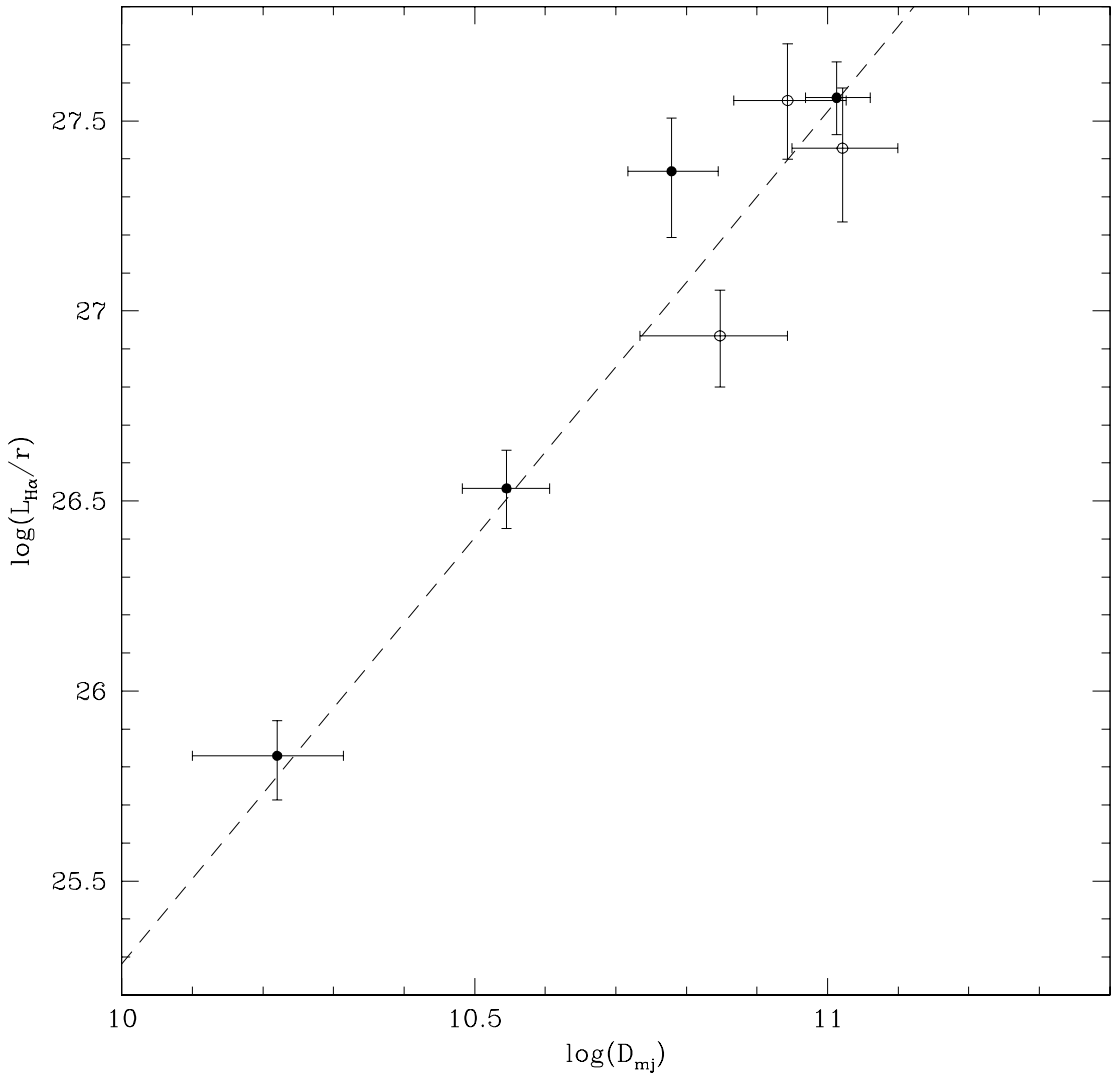

Fig. 11.— Same as Fig. 10, except that the Hα luminosity has been divided by the axial ratio r. A linear fit in the log-log plot produces a best-fit slope of 2.24±0.27 (*dashed line*).

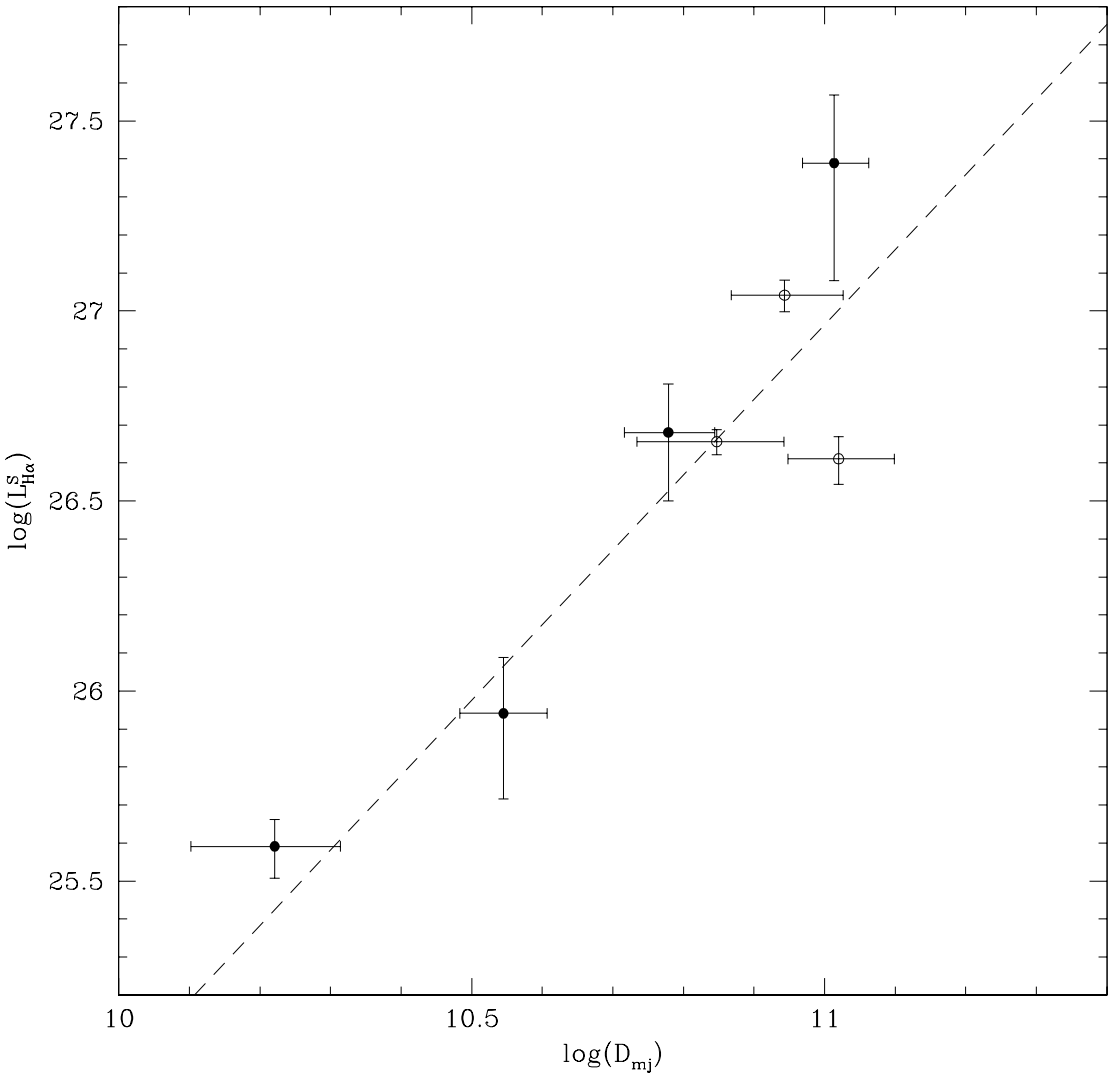

Fig. 12.— Same as Fig. 10, except that the Hα luminosity has been calculated with respect to a synthetic continuum level. A linear fit in the log-log plot produces a best-fit slope of 1.98±0.33 (*dashed line*).

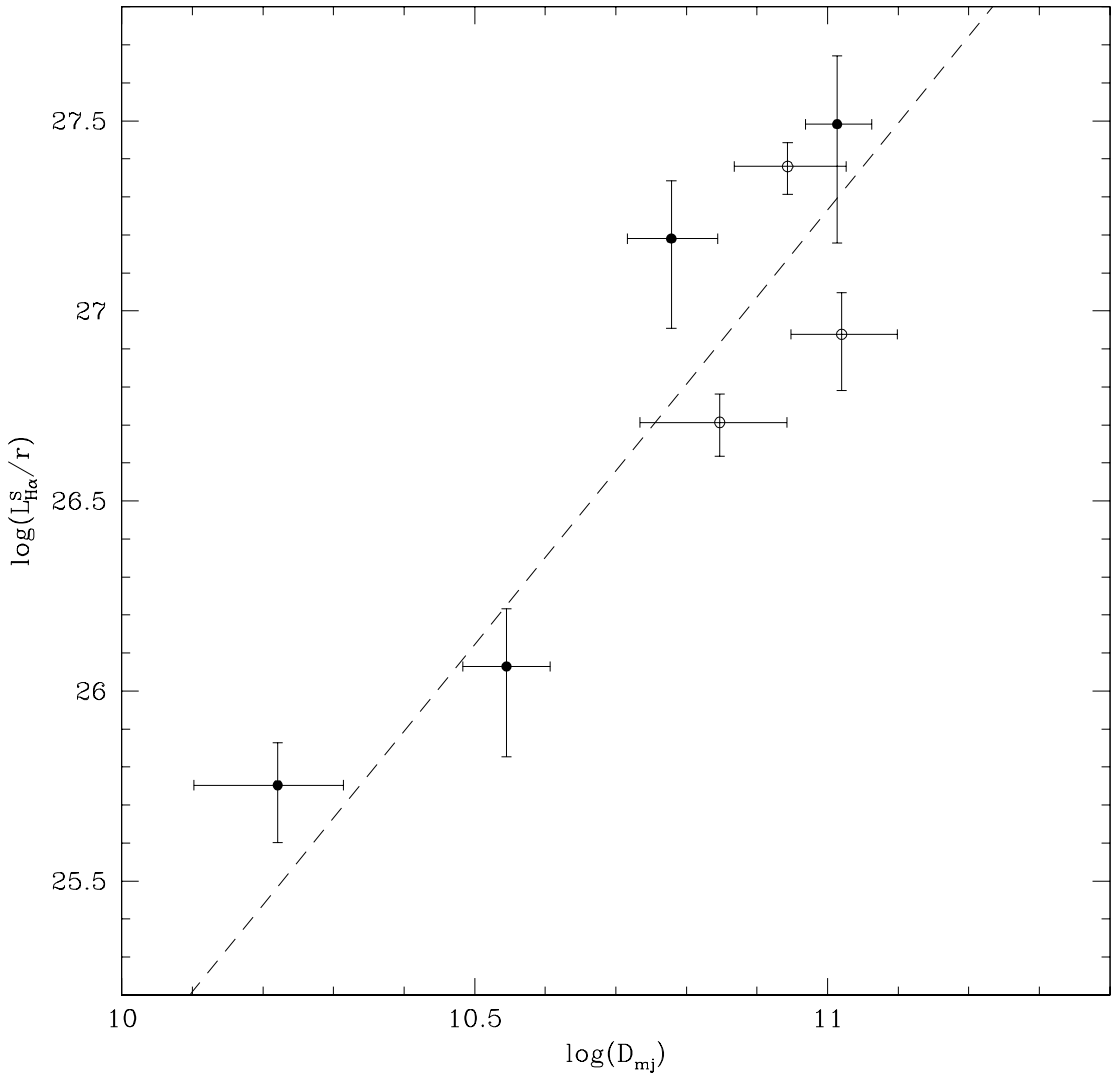

Fig. 13.— Same as Fig. 11, except that the Hα luminosity has been calculated with respect to a synthetic continuum level. A linear fit in the log-log plot produces a best-fit slope of 2.28±0.38 (*dashed line*).

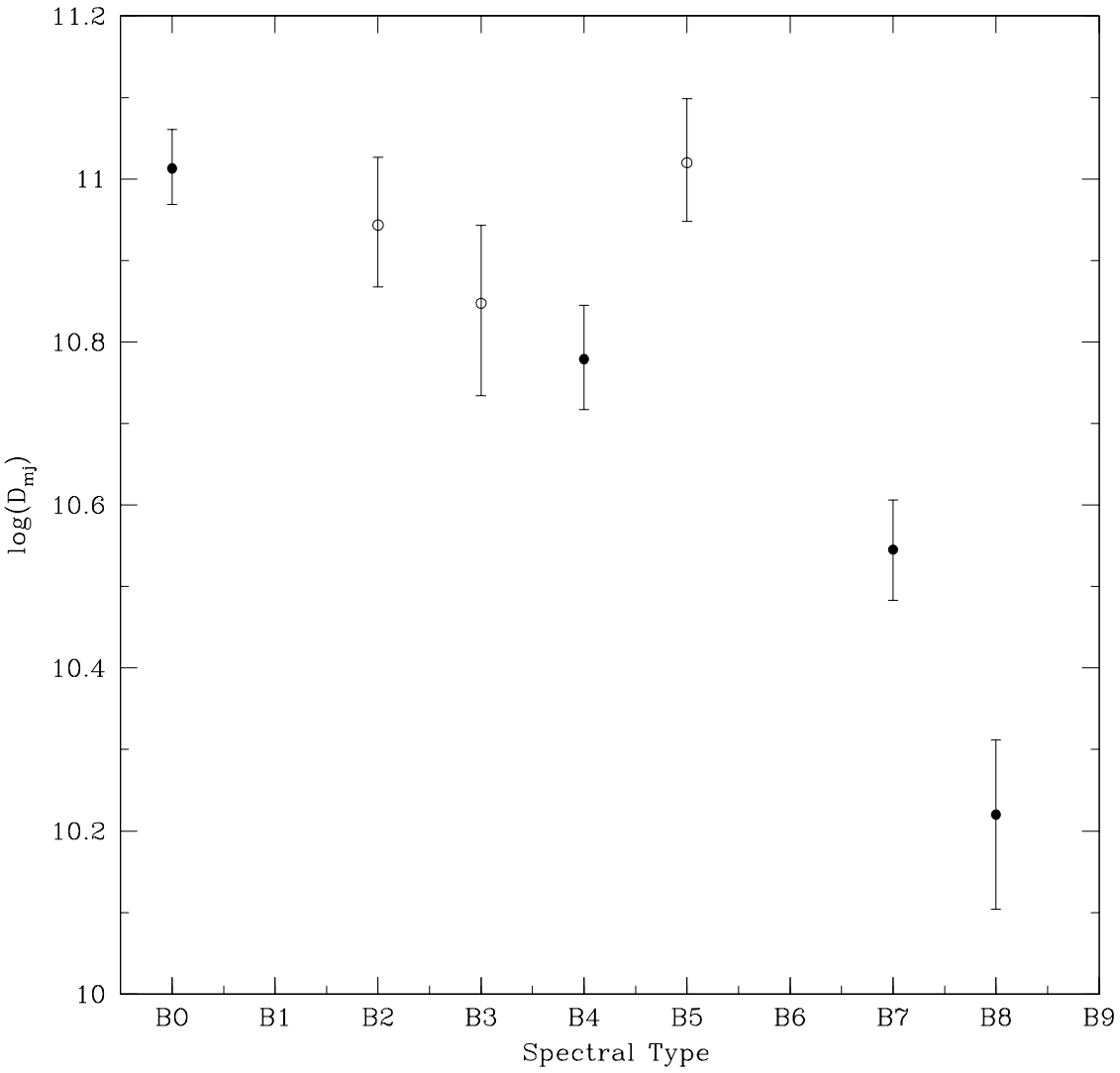

Fig. 14.— The size of the major axis of the disk as a function of the spectral type.

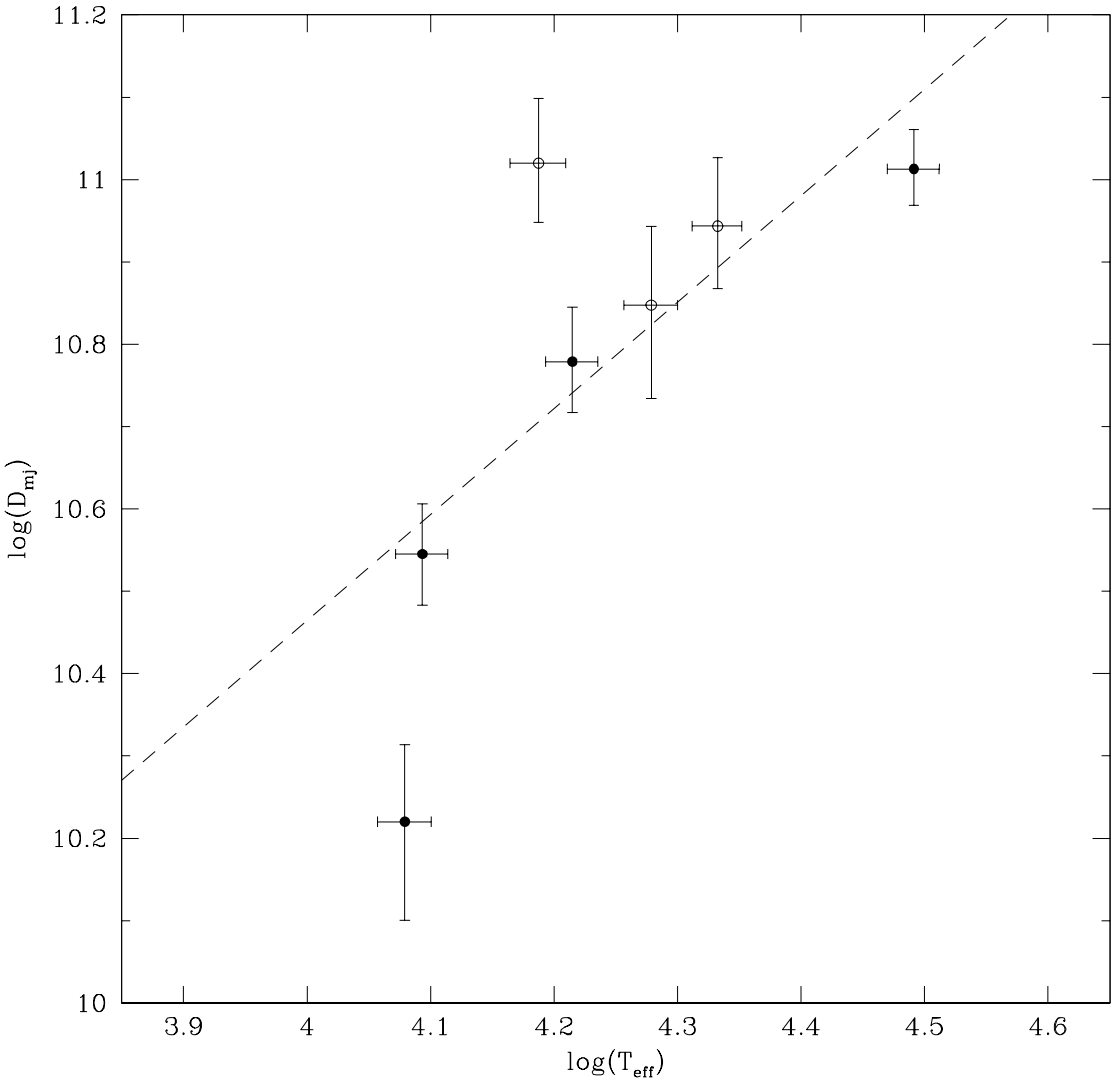

Fig. 15.— The size of the major axis of the disk as a function of the effective temperature of the central star.

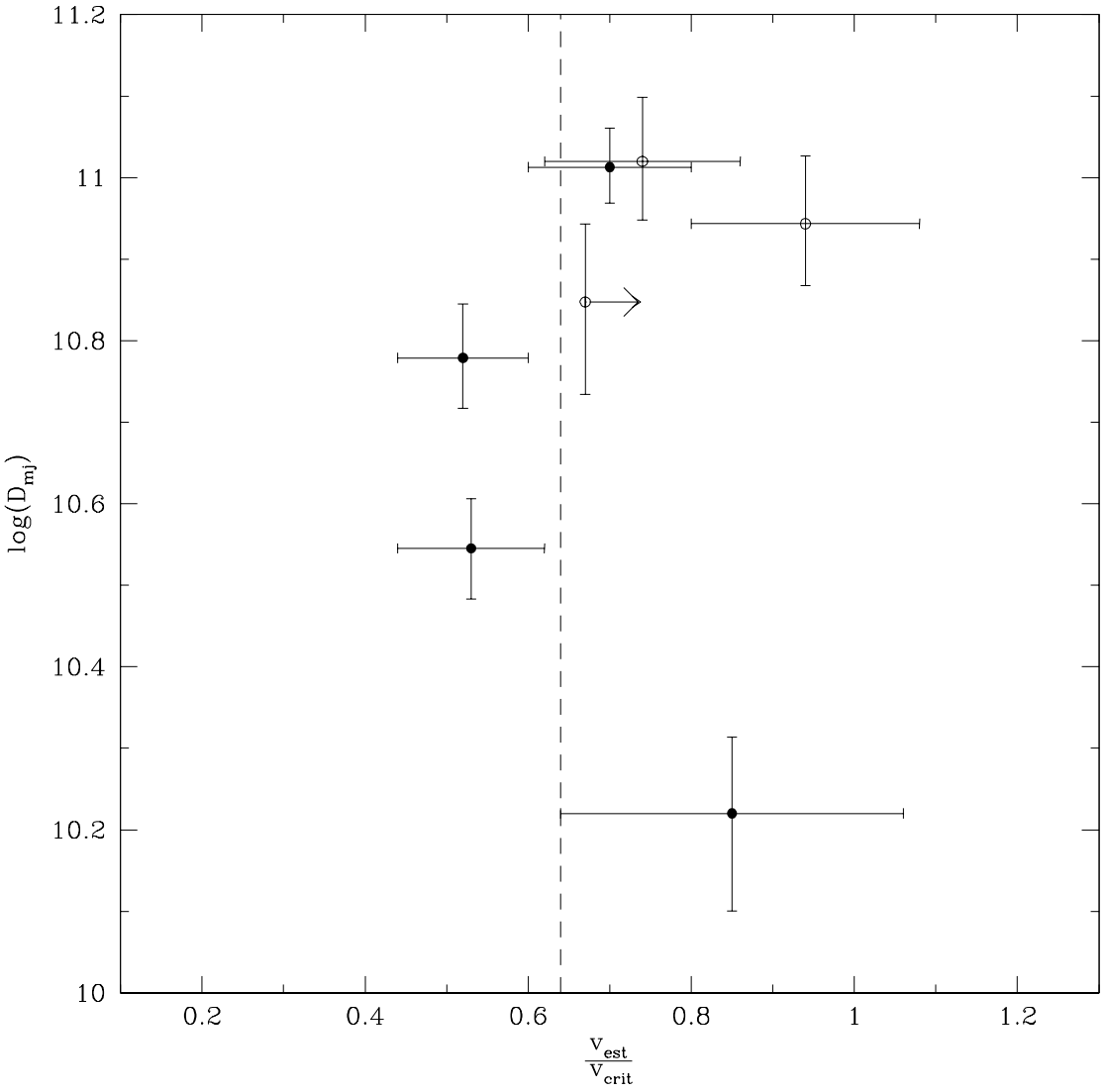

Fig. 16.— The the size of the major axis of the disk as a function of the estimated rotational velocity (in units of critical velocity). The weighted average value of $v_{\rm est}/v_{\rm crit}$ is shown with *dashed line*.